Zinc transporter 2 interacts with vacuolar ATPase and is required for polarization, vesicle acidification, and secretion in mammary epithelial cells

Received for publication, May 3, 2017, and in revised form, September 22, 2017 Published, Papers in Press, November 7, 2017, DOI 10.1074/jbc.M117.794461

Sooyeon Lee[‡1], **Olivia C. Rivera**[‡], **and Shannon L. Kelleher**[‡§¶‖2]

From the Departments of [‡]*Cellular and Molecular Physiology,* [¶]*Pharmacology, and* [§]*Surgery, Penn State Hershey College of Medicine, Hershey, Pennsylvania 17033 and the* [‖]*Department of Nutritional Sciences, The Pennsylvania State University, University Park, Pennsylvania 16802*

Edited by Thomas Söllner

An important feature of the mammary gland is its ability to undergo profound morphological, physiological, and intracellular changes to establish and maintain secretory function. During this process, key polarity proteins and receptors are recruited to the surface of mammary epithelial cells (MECs), and the vesicle transport system develops and matures. However, the intracellular mechanisms responsible for the development of secretory function in these cells are unclear. The vesicular zinc (Zn^{2+}) transporter ZnT2 is critical for appropriate mammary gland architecture, and ZnT2 deletion is associated with cytoplasmic Zn^{2+} accumulation, loss of secretory function and lactation failure. The underlying mechanisms are important to understand as numerous mutations and non-synonymous genetic variation in ZnT2 have been detected in women that result in severe Zn^{2+} deficiency in exclusively breastfed infants. Here we found that ZnT2 deletion in lactating mice and cultured MECs resulted in Zn^{2+}-mediated degradation of phosphatase and tensin homolog (PTEN), which impaired intercellular junction formation, prolactin receptor trafficking, and alveolar lumen development. Moreover, ZnT2 directly interacted with vacuolar H^+-ATPase (V-ATPase), and ZnT2 deletion impaired vesicle biogenesis, acidification, trafficking, and secretion. In summary, our findings indicate that ZnT2 and V-ATPase interact and that this interaction critically mediates polarity establishment, alveolar development, and secretory function in the lactating mammary gland. Our observations implicate disruption in ZnT2 function as a modifier of secretory capacity and lactation performance.

In many highly-specialized eukaryotic cells, secretory function is mediated through regulated vesicle trafficking (1), which first requires the establishment of epithelial cell polarity (2–5). In the mammary gland, mammary epithelial cell (MEC)[3] polarity develops primarily during late pregnancy/early lactation (6, 7) and is characterized by the formation of adherence and tight junctions followed by luminal expansion (reviewed in Refs. 2, 4, and 8). Polarity is critical for both establishing the secretion of milk components into the alveolar lumen and concurrently, limiting the passage of solutes, such as sodium and chloride, from the basolateral bloodstream (9). Several well-described factors involved in polarity establishment, such as phosphatase and tensin homolog (PTEN), cell division control protein homologue 42 (Cdc42), and annexins (2, 10), are critical regulators of MEC integrity and function (3, 11, 12). Second, to complete the development of secretory function, the vesicle secretion system must be established. In neurons and pituitary cells, vesicle secretion is predicated upon vesicle acidification (13–16). This process is dependent upon vacuolar H^+-ATPase (V-ATPase), a proton pump that is responsible for the development of a proton gradient across intracellular membranes (17, 18). We previously showed that V-ATPase is expressed in MECs (19) and more recently, V-ATPase was implicated in mammary gland development (20). However, the specific role of V-ATPase in the mammary gland is not well-understood, and a direct role for V-ATPase in secretion during lactation has not been shown.

Impairments in secretory function can lead to suboptimal lactation (21, 22) or overt lactation failure (23, 24). Emerging evidence suggests that disturbances in mammary gland zinc (Zn^{2+}) homeostasis compromise secretory function (25–30). Zinc is an essential ion that is required by 10% of the eukaryotic proteome and plays a vital role in over 300 cellular processes (*e.g.* transcription, translation, enzyme activity, and intracellular signaling) and cellular functions (*e.g.* proliferation, polarity, apoptosis, and differentiation). One protein that is critical for Zn^{2+} management in the mammary gland is the vesicle Zn^{2+} transporter ZnT2 (*SLC30A2*) (31–33). ZnT2 expression is restricted to highly-specialized secretory tissues, such as the pancreas, prostate, placenta, ovary, and mammary gland (34). ZnT2 has six transmembrane domains (35) and functions as a dimer to transport Zn^{2+} from the cytoplasm into vesicles (30, 32, 33). ZnT2-null mice accumulate cytoplasmic Zn^{2+} in MECs

This work was supported by intramural funds from the Penn State Hershey Department of Surgery (to S. L. K.). The authors declare that they have no conflicts of interest with the contents of this article.

This article contains Figs. S1–S4.

[1] Present address: Dept. of Medicine, Division of Endocrinology, Stanford University School of Medicine, Stanford, CA 94305.

[2] To whom correspondence should be addressed: The University of Massachusetts, 883 Broadway, Lowell, MA 01854. Tel.: 978-934-3527; Fax: 978-934-4704; E-mail: shannon_kelleher@uml.edu.

[3] The abbreviations used are: MEC, mammary epithelial cell; Axn2, annexin 2; Cdc42, cell division control protein 42; PRL, prolactin; PRLR, prolactin receptor; PTEN, phosphatase and tensin homolog; V-ATPase, vacuolar H^+-ATPase; ZnT2, zinc transporter 2; ZO-1, zonula occludens-1; TPEN, *N*,*N*,*N*′,*N*′-tetrakis(2-pyridylmethyl)ethylenediamine; IF, immunofluorescence.

in vivo, which is associated with impaired intracellular organization and reduced STAT5 signaling, leading to defects in mammary gland architecture, impaired secretion, altered milk composition, and lactation failure. This is consistent with reports in ZnT2-attenuated MECs *in vitro*, in which cytoplasmic Zn^{2+} levels are increased and associated with reduced STAT5 activation and secretion. These observations collectively implicate ZnT2 in prolactin receptor (PRLR)-mediated establishment of MEC polarity and secretory function (27).

The identification of several mutations in *SLC30A2*, that reduce milk Zn^{2+} concentration (26, 30, 36, 37) and lead to increased infant morbidity (38, 39), underlies the clinical importance of understanding the role and regulation of ZnT2. Moreover, we recently reported that expression of non-synonymous variants in *SLC30A2* is surprisingly common (29). Studies *in vitro* found that many of these ZnT2 variants result in subcellular Zn^{2+} redistribution and cytotoxic Zn^{2+} accumulation (29, 40). Intriguingly, several ZnT2 variants are associated with elevated milk sodium levels, a hallmark of breast dysfunction during lactation (41–43), implicating defects in ZnT2-mediated intracellular Zn^{2+} management as a modifier of MEC function.

In this study, we hypothesized that ZnT2 plays a direct role in establishing secretory function. We demonstrated that loss of ZnT2-mediated Zn^{2+} transport lead to PTEN degradation and impaired recruitment of apical polarity proteins, which interfered with the proper establishment of polarity and PRLR trafficking to the cell surface. Most interestingly, we found that ZnT2 is critical for V-ATPase assembly and vital for secretory vesicle biogenesis, acidification and secretion.

Results and discussion

Loss of ZnT2 disrupts junction formation and lumen development in the mammary gland in vivo

The mammary glands from lactating ZnT2-null mice have profound defects in secretory function, including a lack of lobulo-alveolar structures and severe disorganization of intracellular vesicles and organelles, which is associated with impaired milk secretion (27). Establishing MEC polarity is important for the development of secretory function and producing adequate milk volume (44–46). In the mammary gland, a primary hallmark of reduced MEC polarity is impaired alveolar expansion (44). Consistent with this, we found that 60% of the mammary gland alveoli in *ZnT2ko* mice failed to expand (Fig. 1, *A* and *B*), as their luminal area was significantly smaller compared with their *wt* littermates (Fig. 1*C*). Key molecules important for MEC polarity are E-cadherin, an adherence junction protein located specifically in the basolateral region, and zonula occludens 1 (ZO-1), a tight junction protein located apico-laterally. Mislocalization of E-cadherin and ZO-1 indicates disrupted intercellular adhesion and apical-basolateral segregation (44). As expected, these proteins were located to their respective subdomain in the mammary epithelia of *wt* mice (Fig. 1*D, i–ii*, and *E, i–iii*). However, in *ZnT2ko* mice, lateral staining of E-cadherin was lacking (Fig. 1*D, iii–iv*), and ZO-1 was retained in discrete cytoplasmic regions in MECs (Fig. 1*E, v–vii*). These defects in intercellular adhesion and lumen development were further revealed at the subcellular level using transmission electron microscopy. Mammary glands from *wt* mice illustrate fully functional and mature alveoli with vastly expanded lumen, which are lined by polarized MECs linked together by intact tight and adherens junctions on the lateral surface (Fig. 1*F, i–ii*). In contrast, *ZnT2ko* mice had poorly expanded alveoli that lacked defined junctions between adjacent cells (Fig. 1*F, iii–iv*). Collectively, this provides compelling evidence that MEC polarity was impaired in the mammary glands of ZnT2-null mice.

ZnT2-mediated Zn^{2+} transport maintains PTEN stability and the development of polarity

Polarity and the establishment of secretory function in MECs are stimulated by PRL (47, 48). To identify mechanisms through which the loss of ZnT2 leads to impairs MEC polarity and lumen development, HC11 cells were cultured on Matrigel® then treated with PRL, and the ability to form 3D mammospheres with mature alveoli was assessed (Fig. 2*A*). ZnT2-expressing MECs formed well-organized mature mammospheres complete with an expanded lumen and appropriate polarization (Fig. 2*B*). In contrast, ZnT2-attenuated cells did not form polarized and mature alveoli (Fig. 2, *C* and *D*) and ~90% of ZnT2KD mammospheres failed to form a lumen in 3D culture (Fig. 2*E*). Consistent with our observations *in vivo*, we found that ZnT2-expressing cells in 2D culture formed intercellular junctions, indicated by the contiguous staining of both E-cadherin (Fig. 2*F*), and ZO-1 at the cell surface (Fig. 2*G*) in response to PRL treatment. In contrast, ZnT2-attenuated cells lacked contiguous cell-surface staining of both E-cadherin and ZO-1. This observation begs the question as to the identity of the primary defect in MECs that lack ZnT2 expression.

In epithelial cells, three major polarity complexes, PAR, Crumbs, and Scribble (10), regulate apical-basolateral organization and asymmetric segregation of the cell membrane, intracellular organelles, and the cytoskeleton (2), and coordinate cell cycle progression (40). Of these major polarity complexes, the PAR complex is the most well-characterized in epithelial cells, and responsible for the recruitment of PTEN to the cell membrane (5, 49, 50). Under normal conditions, cytosolic PTEN translocates to the cell membrane via myosin-based transport machinery (51), where it transiently associates with the cell membrane and acts as a lipid phosphatase to hydrolyze phosphatidylinositol (3,4,5)-triphosphate to phosphatidylinositol (3,5)-diphosphate, antagonizing the PI3K/Akt pathway (50). PTEN-mediated epithelial polarization promotes proper localization of molecular factors and subcellular organelles that allow cells to efficiently respond to secretory differentiation cues for alveolar development (52). During polarity establishment, PTEN directs the enrichment of proteins to the apical membrane by recruiting Axn2, which in turn recruits Cdc42, a small GTPase of the Rho family that regulates signaling pathways that control diverse cellular functions including cell morphology, migration, endocytosis, and cell cycle progression (53). Ultimately this sequence of events activates the PAR complex (49), which is vital for the process of alveologenesis (54). In the mammary epithelium, PTEN exerts these effects through several signaling pathways, such as mitogen-activated protein

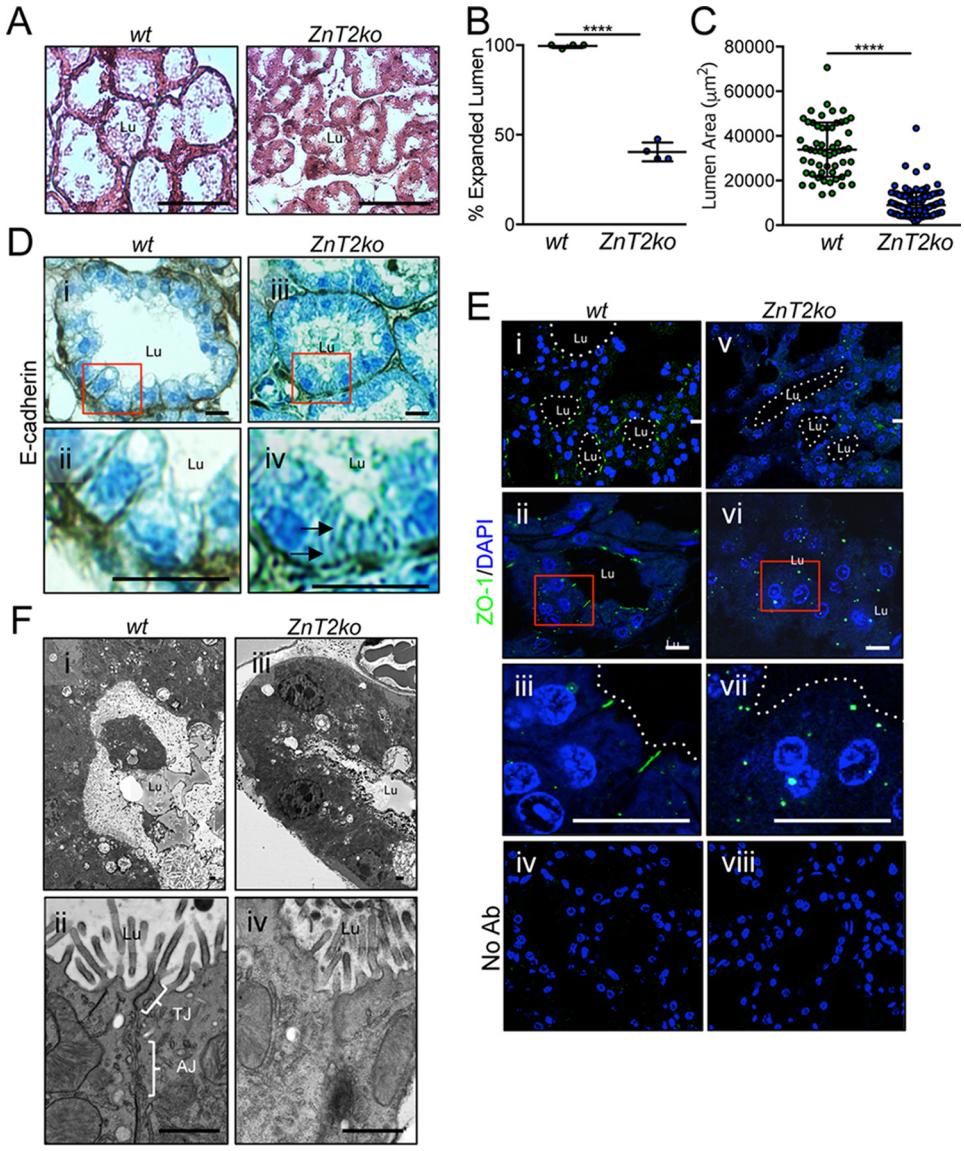

Figure 1. ZnT2-null mice have defects in junction formation and lumen development in the lactating mammary gland. *A,* representative hematoxylin and eosin-stained mammary gland sections illustrating differences in luminal area (*Lu*) in lactating wild-type (*wt*) and ZnT2-null (*ZnT2ko*) mice. *Scale bar*, 100 μm. *B,* data represent mean % of alveoli with expanded lumen ± S.D. in five random images (×10) from 4 mice/genotype; ****, $p < 0.0001$. *C,* data represent mean luminal area (μm^2) ± S.D. in *wt* ($n = 129$ alveoli) and ZnT2*ko* ($n = 362$ alveoli) mice from 4 mice/genotype; ****, $p < 0.0001$. *D,* representative images of E-cadherin staining in mammary gland sections from *wt* and *ZnT2ko* mice. *Box outlines* the area illustrated by the zoomed images (*ii* and *iv*). Note the lack of distinct E-cadherin staining between cells (*arrow*) in *ZnT2ko* mice. *Scale bar*, 20 μm. *E,* representative images of ZO-1 staining (*green*) in mammary gland sections from *wt* and *ZnT2ko* mice. Nuclei were counterstained with DAPI (*blue*). *Box outlines* the area illustrated by the zoomed images (*iii* and *vii*). No Ab sections were incubated without primary antibody as a negative control (*iv* and *viii*). Note the lack of ZO-1 staining at the membrane and the puncta detected in the cytoplasm of the MECs. *Scale bar*, 20 μm. *F,* representative transmission electron micrographs showing luminal expansion (*i* and *iii*) and intercellular junctions (*ii* and *iv*) in mammary gland tissue from *wt* (*i* and *iii*) and *ZnT2ko* (*ii* and *iv*) mice. Note the constricted lumen and lack of defined intercellular junctions in the mammary glands of *ZnT2ko* mice. *Scale bar*, 1 μm. *Lu*, alveolar lumen; *TJ*, tight junction; *AJ*, adherens junction.

kinases (MAPK), focal adhesion kinase (FAK), and PI3K-AKT, playing a critical role in mammary development and lactation (55, 56). Loss of PTEN expression inhibits cell polarization, functional differentiation, and tissue development (57–59). In addition, PTEN is one of the most frequently mutated proteins in human cancers and loss of PTEN expression promotes tumor formation (60–62). Consequently, understanding the molecular mechanisms regulating PTEN expression and function are undoubtedly critical for the prevention of and intervention in multiple pathologies associated with the loss of cell polarity.

Relative to mammary glands and HC11 cells expressing ZnT2, PTEN expression was significantly reduced by ~30% in the mammary glands of *ZnT2ko* mice (Fig. 3, *A* and *B*), and by ~50% in ZnT2-attenuated cells (Fig. 3, *D* and *E*, Fig. S1). Because PTEN inhibits AKT activation (63), we used AKT activation as readout to confirm that PTEN activity was repressed. Indeed, we found that AKT activation was enhanced in the mammary glands of *ZnT2ko* mice (Fig. 3*C*) and in ZnT2KD cells (Fig. 3*F*), verifying functional consequences of PTEN degradation. Studies in neurons and airway epithelial cells show that Zn^{2+} induces PTEN degradation through the ubiquitin-

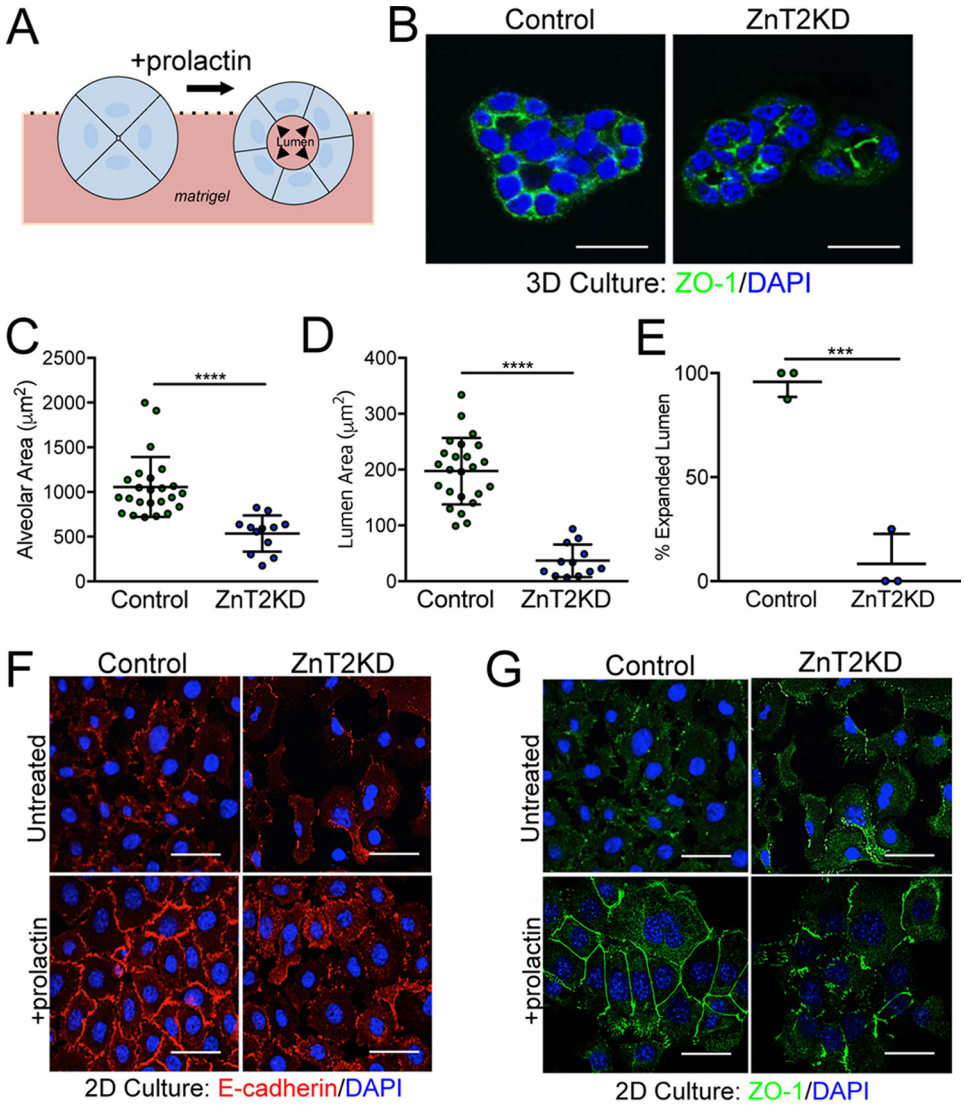

Figure 2. Loss of ZnT2 disrupts lumen development by impairing MEC polarity *in vitro*. *A,* schematic model of PRL-stimulated lumen development in 3D culture. *B,* representative confocal images of ZO-1 staining (*green*) in ZnT2-expressing (*Control*) and -attenuated (ZnT2KD) cells grown in 3D culture. Nuclei were counterstained with DAPI (*blue*). Note the collapsed lumen in ZnT2KD mammospheres. *Scale bar,* 20 μm. *C,* data represent mean luminal area (μm^2) ± S.D. in 23 (*Control*) or 12 (*ZnT2KD*) intact mammospheres identified in three independent experiments; ****, $p < 0.0001$. *D,* data represent mean luminal diameter (μm) ± S.D. in 23 (*Control*) or 12 (*ZnT2KD*) intact mammospheres identified in three independent experiments; ****, $p < 0.0001$. *E,* data represent mean % of mammospheres with expanded luminal area ± S.D. from five random images (×10)/group from three independent experiments; ***, $p < 0.001$. *F* and *G,* representative confocal images of E-cadherin (*F, red*) and ZO-1 (*G, green*) in mock-transfected (*Control*) and ZnT2-attenuated (*ZnT2KD*) cells grown in 2D culture and either treated with prolactin for 24 h or left untreated. Nuclei were counterstained with DAPI (*blue*). Note the non-contiguous staining of E-cadherin and ZO-1 on the periphery of ZnT2KD cells. *Scale bars*, 20 μm.

proteasome pathway (63, 64). Importantly, we previously showed that cytoplasmic Zn^{2+} accumulates in the MECs of lactating ZnT2-null mice and in ZnT2-attenuated MECs cultured *in vitro* (27). This led us to hypothesize that cytoplasmic Zn^{2+} accumulation in ZnT2-attenuated MECs is the factor behind reduced PTEN expression and disruption of polarity establishment. To test this, we briefly treated ZnT2-attenuated MECs with a modest amount of the Zn^{2+} chelator *N,N,N′,N′*-tetrakis(2-pyridylmethyl)ethylenediamine (TPEN) and found that PTEN abundance was indeed restored (Fig. 3, *G* and *H*). A possible mechanism by which the loss of ZnT2 leads to Zn^{2+}-mediated PTEN degradation may be through ubiquitination and proteasomal degradation (63). To test this hypothesis, ZnT2-expressing and ZnT2-attenuated cells were pretreated with the proteasome-specific inhibitor MG132, and PTEN protein abundance was evaluated by immunoblotting. As previously discussed, ZnT2 attenuation significantly decreased PTEN abundance. In comparison, pretreatment with MG132 blocked the loss of PTEN in ZnT2-attenuated cells (Fig. 3, *I* and *J*) and reduced AKT activation (Fig. 3*K*). Taken together, these results indicate that the loss of ZnT2-mediated Zn^{2+} transport into intracellular vesicles increases cytoplasmic Zn^{2+} and PTEN degradation through the proteasomal pathway in MECs.

We next examined membrane recruitment of key polarity factors downstream of PTEN activity. In ZnT2-expressing cells, Axn2 staining could be observed at the cell periphery, indicating successful membrane recruitment by PTEN (Fig. 4*A*). However, Axn2 was retained proximal to the nucleus and failed to traffic to the membrane in ZnT2-attenuated MECs. This was confirmed by the loss of Axn2 co-localization with PKH26, a

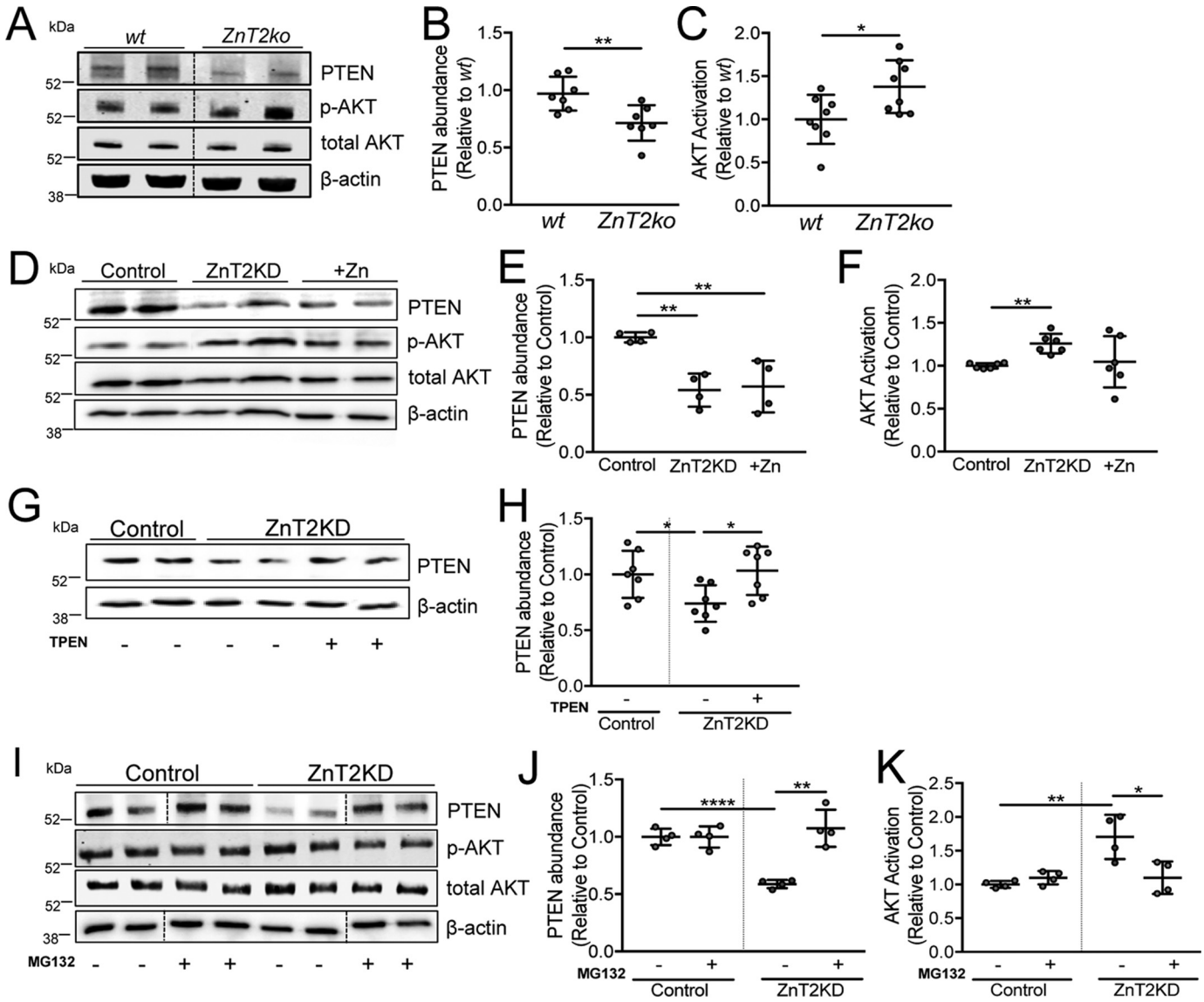

Figure 3. ZnT2-mediated Zn^{2+} transport regulates PTEN stability in MECs *in vitro*. *A,* representative immunpblot of PTEN, *p*-AKT, and total AKT in lysates from wild-type (*wt*) and ZnT2-null (*ZnT2ko*) mammary glands. β-Actin served as a loading control. *Dotted lines* indicate spliced sections obtained from a single immunoblot; representative samples ($n = 2$/group) were selected for publication. *B,* data represent the mean PTEN/β-actin ratio relative to *wt* ± S.D., $n = 7$ mice/genotype; **, $p < 0.01$. *C,* data represent mean *p*-AKT/total AKT ratio relative to *wt* ± S.D., $n = 7$ mice/genotype; *, $p < 0.05$. *D,* representative immunoblot of PTEN, *p*-AKT, and total AKT in cell lysates of mock-transfected (*Control*), ZnT2-attenuated (*ZnT2KD*), and Zn^{2+}-treated (+*Zn*) cells. β-Actin served as a loading control. *E,* data represent mean PTEN/β-actin ratio relative to control ± S.D., $n = 4$ samples/group; **, $p < 0.01$. *F,* data represent mean *p*-AKT/total AKT ratio relative to control ± S.D., $n = 6$ samples/group; **, $p < 0.01$. *G,* representative immunoblot of PTEN in cell lysates of control and ZnT2KD cells pre-treated with (+) or without (−) 10 μM TPEN for 2 h. β-Actin served as a loading control. *H,* data represent mean PTEN/β-actin ratio relative to control ± S.D., $n = 7$ samples/group; *, $p < 0.05$. *I,* representative immunoblot of PTEN in cell lysates from control and ZnT2KD cells pre-treated with (+) or without (−) 10 μM MG132 for 3 h. β-Actin served as a loading control. *Dotted lines* indicate spliced sections obtained from a single immunoblot; sample order was changed for labeling consistency. *J,* data represent mean PTEN/β-actin ratio relative to control ± S.D., $n = 4$ samples/group; **, $p < 0.01$ and ****, $p < 0.0001$. *K,* data represent mean *p*-AKT/total AKT ratio relative to control ± S.D., $n = 4$ samples/group; *, $p < 0.05$ and **, $p < 0.01$. All spliced images were from a single immunoblot.

cell membrane maker, in ZnT2-attenuated cells (Fig. 4, *B* and *C*). Similarly, Cdc42 was primarily detected in the membrane fraction isolated from ZnT2-expressing cells (Fig. 4*D*), whereas, in contrast, Cdc42 was more evenly distributed between the cytosolic and membrane fractions in ZnT2-attenuated MECs. Disrupted membrane recruitment of Axn2 and Cdc42 implies the loss of asymmetric segregation, which is a key feature for epithelial polarization (3).

The loss of polarity may result in numerous deleterious consequences including receptor trafficking and degradation (65). We previously reported that the mammary glands of lactating ZnT2-null mice and ZnT2-attenuated MECs had reduced STAT5 activation (27). Because PRL binding to PRLR on the cell surface activates Jak2/STAT5 signaling and regulates mammary gland differentiation, milk production, and secretion during lactation (66), we hypothesized that impaired secretory function resulting from the loss in polarity is due to a failure to respond appropriately to PRL. Both confocal imaging (Fig. 4*E*) and cell-surface biotinylation studies (Fig. 4, *F* and *G*) confirmed that PRLR was detected on the cell surface in ZnT2-expressing cells; however, PRLR was absent from the cell surface and instead, was retained proximal to the nucleus in

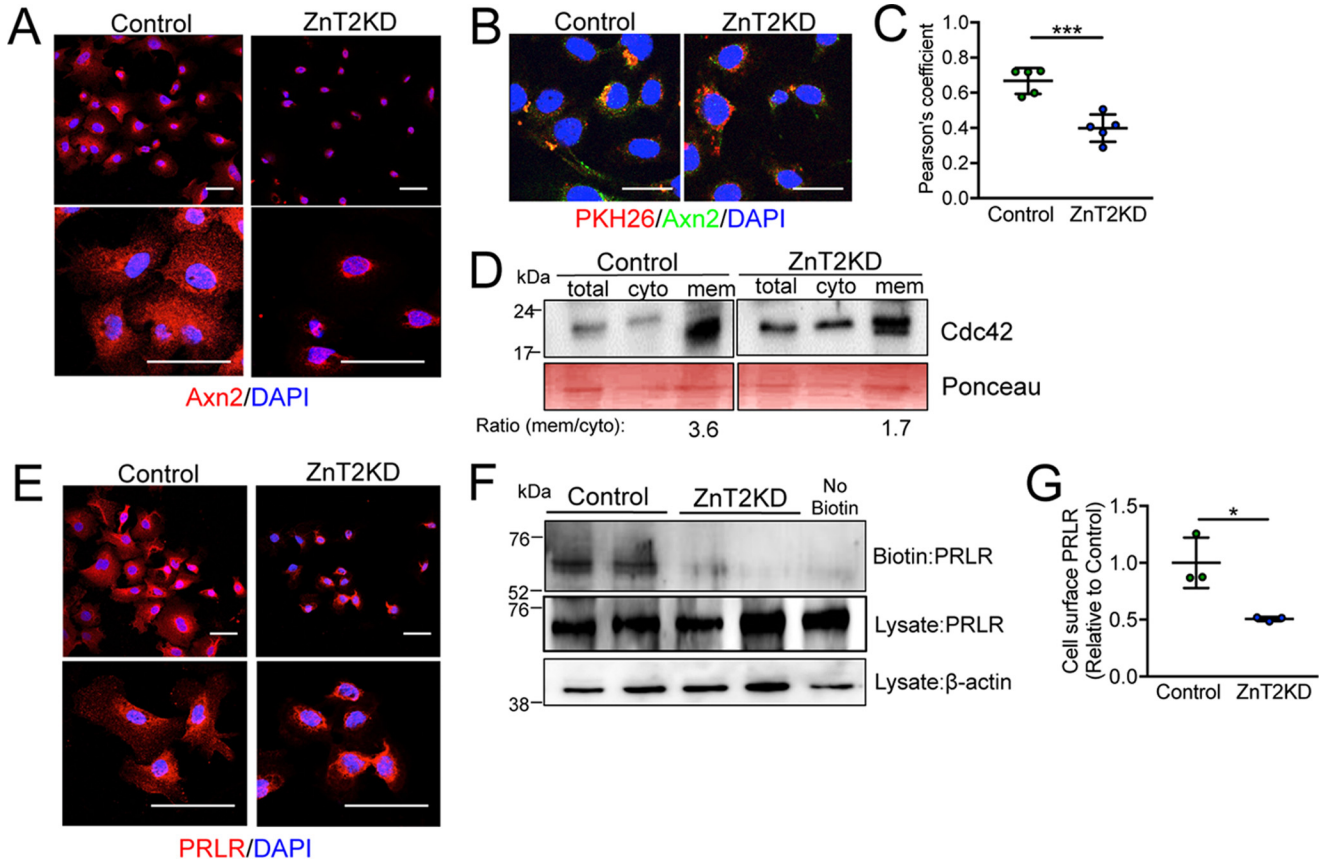

Figure 4. Loss of ZnT2 disrupts membrane recruitment of polarity proteins and PRLR *in vitro*. *A,* representative confocal images of annexin 2 (Axn2, *red*) in mock-transfected (*Control*) and ZnT2-attenuated (*ZnT2KD*) cells. *Scale bar*, 20 μm. Note perinuclear staining of Axn2 in ZnT2KD cells. *B,* representative confocal images of the lipophilic stain PKH26 (*red*) and Axn2 (*green*), illustrating co-localization (*yellow*). Nuclei were counterstained with DAPI (*blue*). *Scale bar*, 20 μm. *C,* data represent mean Pearson's coefficient $\pm$ S.D. calculated from all cells observed in five images ($\times$63)/group; ***, $p < 0.001$. *D,* representative immunoblot of Cdc42 in total, cytosolic (*cyto*), and membrane (*mem*) fractions from control and ZnT2KD cells. Ponceau stain served as loading control. Note the lower ratio of membrane/cytosolic Cdc42 in ZnT2KD cells. *E,* representative confocal images of PRLR (*red*) in control and ZnT2KD cells. Nuclei were counterstained with DAPI (*blue*). *Scale bar*, 20 μm. Note perinuclear staining of PRLR in ZnT2KD cells. *F,* representative immunoblot of PRLR on the cell surface (*Biotin*) and in the cell lysate (*Lysate*) from control and ZnT2KD cells. PRLR in the cell lysate served as normalization control and β-actin in cell lysate served as loading control. A non-biotinylated sample (*No Biotin*) was used as a negative control. *G,* data represent mean cell-surface PRLR/β-actin ratio relative to control $\pm$ S.D., in 2 samples/group from three independent experiments, *, $p < 0.05$.

ZnT2-attenuated cells. Collectively, this demonstrates that the loss of ZnT2 impairs polarity and disrupts PRLR trafficking to the cell surface, which is consistent with impaired PRL signaling and defects in mammary gland differentiation and secretion that we previously observed (27). Interestingly, we previously reported that PRL increases ZnT2 expression (67). Our observations herein suggest that whereas PRL signaling is required to induce ZnT2 expression, ZnT2 is required to appropriately traffic PRLR to the cell surface to further facilitate PRL signaling in the MECs. Collectively this illustrates the importance of ZnT2 in mammary gland function. Moreover, our observations suggest that ZnT2 dysfunction may impair the overall process of membrane protein trafficking; however, further studies are required to explore this possibility.

Loss of ZnT2 disrupted V-ATPase assembly in the mammary gland in vivo

Following polarity establishment, secretory function is fully achieved when the secretion pathway is activated to deliver cargo to and across the cell membrane (1). In the mammary gland, the MECs actively synthesize copious amounts of caseins and other milk constituents that are secreted into the alveolar lumen, primarily by exocytosis (68). Vesicle acidification is required for exocytosis in other specialized secretory tissues, such as the pancreas (69), intestine (70), prostate (71), brain (72), and salivary gland (73). To generate acidified vesicles, V-ATPase functions as a proton pump to transport protons into the vesicular lumen (17). V-ATPase is a multisubunit complex that is composed of two domains, the cytoplasmic V1 domain and the membrane-bound V0 domain (74, 75) that assemble and transport protons upon activation (76). We previously reported that V-ATPase is expressed in the mammary gland (25), and a recent study indicates that deletion of the V-ATPase subunit V0a2 in mice interferes with TGFβ and Notch signaling, compromising mammary gland development during puberty. Moreover, deletion of V0a2 was also associated with lactation defects, which was assumed to be from morphological defects acquired during development (20). Another possibility is that the lack of V-ATPase activity leads to lactation-specific consequences, as vesicle acidification is required for the secretory function of other specialized secretory tissues (13–16, 18). To first provide evidence that V-ATPase plays a specific role in lactation, we showed that expression of the primary membrane-associated regulatory subunit V0a was ~2-fold

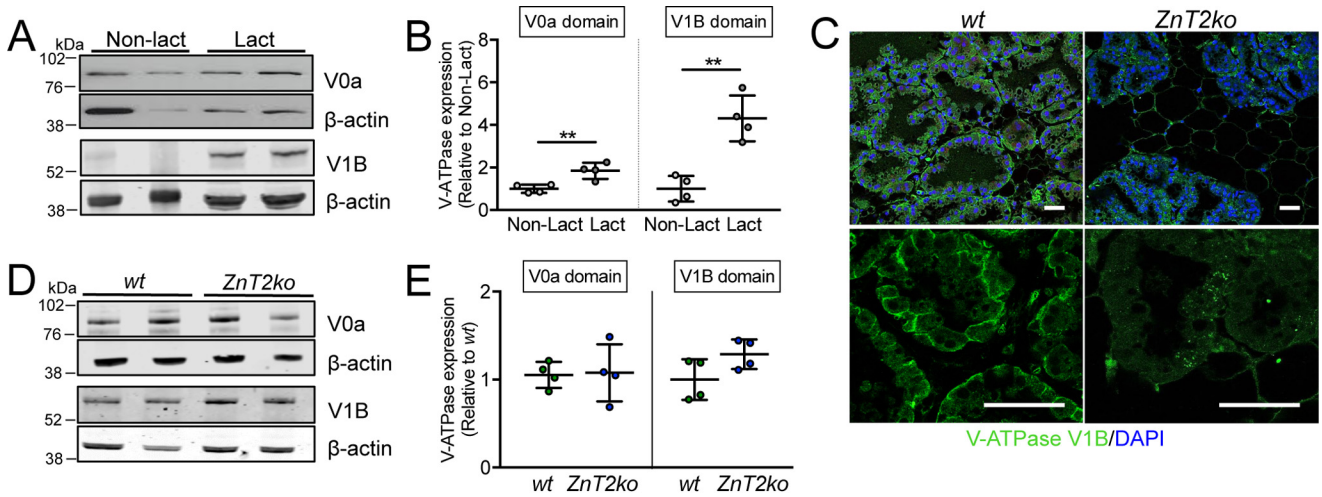

Figure 5. Loss of ZnT2 affects V-ATPase assembly in the mammary gland. *A,* representative immunoblot of V0a and V1B subunits of V-ATPase in lysates from non-lactating (*Non-lact*) and lactating (*Lact*) mouse mammary glands. β-Actin served as a loading control. *B,* data represent mean V0a or V1B/β-actin ratio relative to Non-lact ± S.D., $n = 4$ mice/group; **, $p < 0.01$. *C,* representative images of V1B (*green*) in mammary gland sections from lactating wild-type (*wt*) and ZnT2-null (*ZnT2ko*) mice. Nuclei were counterstained with DAPI (*blue*). Note the membrane staining of V1B in the mammary glands of *wt* mice and the punctate staining of V1B in *ZnT2ko* mice. Magnification, ×20 (*top*), ×63 (*bottom*). *Scale bar*, 50 μm. *D,* representative immunoblot of V0a and V1B subunits in lysates from *wt* and *ZnT2ko* mammary glands. *E,* data represent mean V0a or V1B/β-actin ratio relative to *wt* ± S.D., $n = 4$ mice/genotype.

greater and cytoplasmic-associated subunit V1B was ~3-fold greater in the lactating mammary gland compared with that in nulliparous mice (Fig. 5, *A* and *B*). We next reasoned that if vesicle acidification is an important component of lactation, then the cytoplasmic regulatory subunit V1B would be associated with vesicle membranes to promote V-ATPase assembly and proton transport. Indeed, this is what was observed in *wt* mice (Fig. 5*C*), indicating that V-ATPase assembly, and thus proton transport, was activated. In contrast, we found that in *ZnT2ko* mice, V1B was retained in the cytoplasm and possibly accumulated in large distinct puncta. It is important to note that this difference occurred despite the lack of an effect on total protein level of either V-ATPase domains (Fig. 5, *D* and *E*), indicating that the loss of ZnT2 affected V-ATPase assembly.

ZnT2 is required for the formation of acidified vesicles and secretion in MECs

Similar to what we observed in the mammary glands of lactating mice, MECs that were fully differentiated to secrete following treatment with PRL for 24 h also had significantly greater expression of the subunit V0a (but not V1B) compared with non-secreting MECs (Fig. 6, *A* and *B*). This suggests that although PRL may be a primary regulator of V0a, V1B is regulated by other lactogenic factors that remain to be identified. We previously showed that ZnT2-null mice had defects in secretion (27), and that ZnT2-attenuated MECs were unable to generate acidic vesicles (lysosomes) in response to TNFα stimulation (19); however, it remains unclear as to if, and how the loss of ZnT2 impairs vesicle acidification. To address this gap in knowledge, we first showed that ZnT2 was co-localized with assembled V-ATPase (Fig. 6*C*). Moreover, we found a direct interaction between ZnT2 and V-ATPase under basal, unstimulated conditions, as both the V0a and V1B subunits were detected in ZnT2 immunoprecipitates from non-secreting MECs (Fig. 6*D*, Fig. S2). This interaction was confirmed by the detection of ZnT2 in both V0a and V1B immunoprecipitates, separately (Fig. 6, *E* and *F*). Importantly, we found that the interaction between ZnT2 and V-ATPase (both V0a and V1B subunits) was enhanced in MECs that were differentiated with PRL to form a secreting MEC (Fig. 6, *G* and *H*), providing compelling evidence that ZnT2 and V-ATPase cooperate to promote vesicular Zn^{2+} and proton accumulation for secretion in MECs.

We next measured vesicle acidification directly, using Lysosensor Blue/Yellow DND-160. As a positive control, cells were treated for 5 min with 5 mM glucose, which is known to stimulate V-ATPase-dependent acidification (77). The significant reduction in vesicular pH (from pH 5.4 to 5.0) following glucose treatment validated our tool for measuring vesicle acidification in MECs (Fig. 7, *A* and *B*). Several important findings were made. Importantly, and consistent with a key role for vesicular acidification in secretion in MECs, we found that the vesicular pH was significantly lower in MECs treated with PRL compared with non-secreting MECs (Fig. 7, *A–D*), providing the first evidence that secretory vesicles in MECs become acidified during differentiation. In addition, the size and number of acidic vesicles in PRL-treated cells were significantly greater (Fig. 7, *C–F*), consistent with a role for PRL in vesicle biogenesis and establishing the vesicle secretory system. We noted that ZnT2-attenuation in isolation had a minimal effect on vesicular pH in non-secreting cells; however, the effect of PRL on increasing vesicle acidification was abolished in ZnT2-attenuated MECs (Fig. 7, *C* and *D*). It is important to note that this difference occurred despite no change in total protein level of either V-ATPase domains (Fig. S3). Moreover, ZnT2-attenuation significantly reduced vesicle size (~50%), slightly reduced vesicle number (~25%), and impaired the ability of PRL to activate vesicle biogenesis (Fig. 7, *E* and *F*), providing evidence that ZnT2 is critical for secretory vesicle biogenesis. Vesicular Zn^{2+} has been previously shown to regulate V-ATPase function and acidification in gastric parietal cells and kidney epithelial cells (78, 79). It has

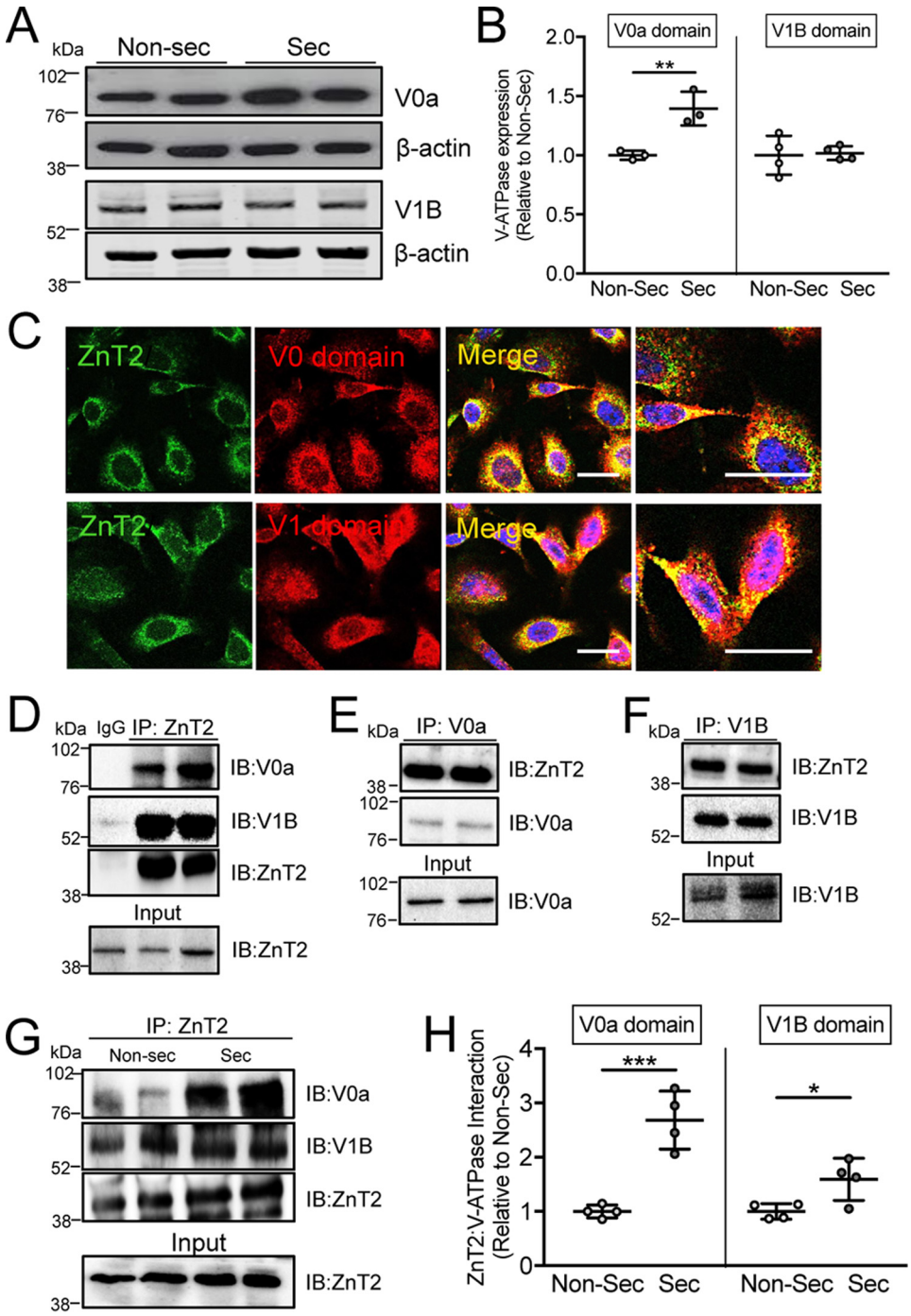

Figure 6. ZnT2 interacts with both V0 and V1 subunits of V-ATPase. *A,* representative immunoblot of V0a and V1B subunits of V-ATPase in lysates from non-secreting (*Non-sec*) and secreting (*Sec*) MECs. *β*-Actin served as a loading control. *B,* data represent mean V0a or V1B/*β*-actin ratio relative to Non-sec ± S.D., $n = 4$ samples/group; **, $p < 0.01$. *C,* representative confocal images of ZnT2 (*green*) and V0a (*red*) or V1B (*red*) in non-secreting MECs. Merged images illustrate co-localization of ZnT2 and the V1 and V0 subunits (*yellow*). *Scale bar*, 20 μm. *D–F*, representative immunoblots of ZnT2, V0a, and V1B in immunoprecipitates (*IP*) from non-secreting MECs. Respective proteins were detected in cell lysates as an input control (*Input*). IgG served as a negative control. *G,* representative immunoblots of V0a, V1B, and ZnT2 in IP of Non-sec and secreting (*Sec*) MECs. ZnT2 in cell lysates served as an input control (*Input*). ZnT2 detected by immunoblotting (*IB*) served as a loading control. *H,* data represent mean V0a or V1B/*β*-actin relative to Non-sec cells ± S.D. in 2 samples/group from four independent experiments, *, $p < 0.05$ and ***, $p < 0.001$.

been reported that Zn^{2+} accumulation interferes with V-ATPase activity (80). Therefore we treated cells with PRL, exposed them to a small amount of the Zn^{2+} chelator TPEN, and then measured vesicle pH. Once again, we found that ZnT2-attenuated cells lost the ability to activate vesicle acidification in response to PRL. Importantly, the presence of TPEN did not remediate this effect (Fig. 7, *G* and *H*). This suggests that the role of ZnT2 in PRL-stimulated vesicle acidification and biogenesis may be independent of its function in Zn^{2+} transport. Although the mechanisms are not yet understood, PRL likely regulates numerous transcription factors, cell cycle proteins, miRNAs, and lipid mediators that are critical for vesicle biogen-

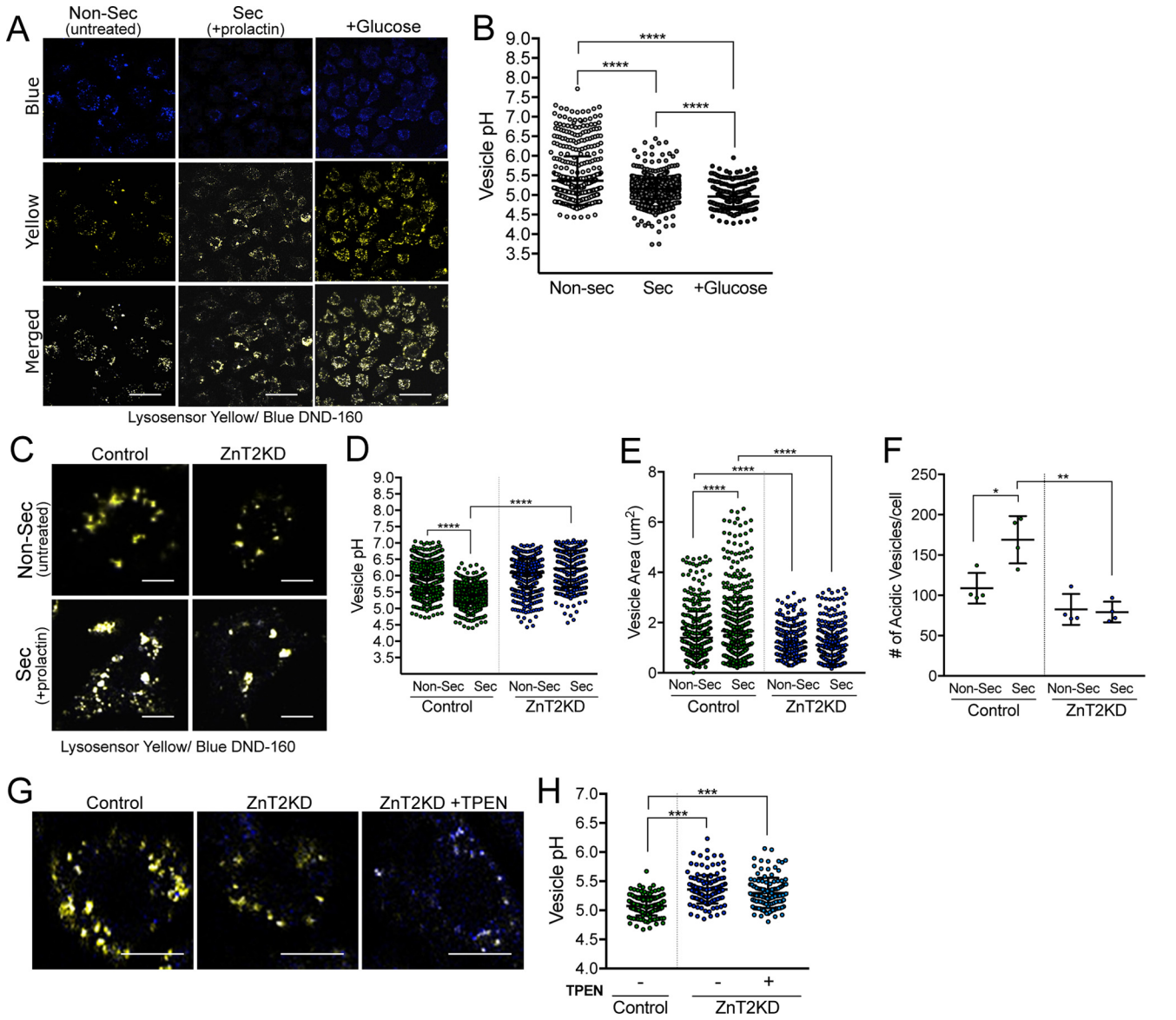

Figure 7. ZnT2-attenuation impairs vesicle acidification and biogenesis in MECs. *A,* representative confocal images of Lysosensor Yellow/Blue DND-160 in non-secreting (*Non-Sec*; *Untreated*) and secreting (*Sec*; *+prolactin*) MECs. Cells were treated with 5 mM glucose (*+Glucose*) for 5 min at 37 °C as a positive control. Both blue and yellow fluorescence intensity was measured. *Scale bar*, 20 μm. *B*, data represent mean vesicular pH ± S.D. of all vesicles from all cells observed in five random images (×63)/group from 4 independent experiments; ****, $p < 0.0001$. *C*, representative confocal images of Lysosensor Yellow/Blue DND-160 in untransfected (*Control*) and ZnT2-attenuated (*ZnT2KD*) cells treated with (*Sec*) or without (*Non-Sec*) prolactin for 24 h. *Scale bar*, 20 μm. *D,* data represent mean vesicular pH ± S.D. of all vesicles from all cells observed in five random images (×63)/group from 4 independent experiments; ****, $p < 0.0001$. *E,* data represent mean vesicle area (μm^2) ± S.D. of all vesicles from all cells observed in five random images (×63)/group from 4 independent experiments; ****, $p < 0.0001$. *F,* data represent mean number of vesicles/cell ± S.D. from all cells in five random images (×63)/group from 4 independent experiments; *, $p < 0.05$ and **, $p < 0.01$. *G,* representative high magnification confocal images of one secreting MEC (*i.e.* pretreated with PRL for 24 h) that was untransfected (*Control*), ZnT2-attenuated (*ZnT2KD*), or ZnT2-attenuated and then treated with TPEN (*ZnT2KD+TPEN*) or with Lysosensor Yellow/Blue DND-160. *Scale bar*, 10 μm. *H,* data represent mean vesicular pH ± S.D. of all vesicles in all cells from five random images (×63)/group; ***, $p < 0.001$.

esis (81, 82), which may be impaired by the loss of ZnT2. Further studies are required to determine the molecular interaction between ZnT2 and V-ATPase, and mechanisms through which ZnT2 regulates vesicle biogenesis and acidification in MECs.

Polarized MECs actively synthesize copious amounts of caseins and other milk constituents (83–85) that are packaged into vesicles for secretion into the alveolar lumen by exocytosis (68). We reasoned that if vesicle acidification is important for vesicle secretion in MECs, then V-ATPase should co-localize with major milk proteins, and impaired acidification should reduce vesicle secretion. Indeed we found that V-ATPase and β-casein were largely co-localized in secretory vesicles (Fig. 8*A*). However, in ZnT2-attenuated MECs, V-ATPase and β-casein were significantly less co-localized (Fig. 8*B*), consistent with a role for ZnT2 as an interacting partner of V-ATPase in secretory vesicle biogenesis and secretion. To determine whether the loss of ZnT2 affects vesicle secretion directly, we transfected cells with GFP-tagged β-casein and found that although ZnT2-expressing cells successfully formed and trafficked β-casein-containing vesicles toward the cell surface in response to PRL, β-casein was retained in the perinuclear

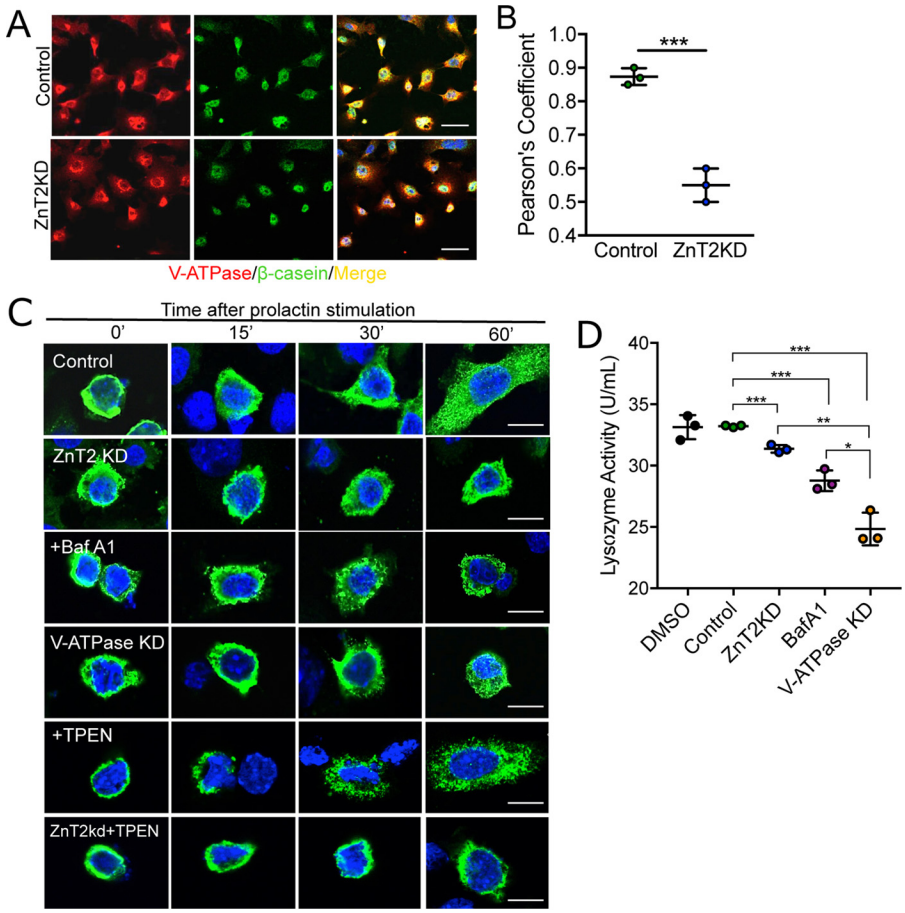

Figure 8. Secretory functions are impaired in ZnT2-attenuated MECs. *A,* representative confocal images of V-ATPase (V0a; *red*) and β-casein (*green*) in mock-transfected (*Control*) and ZnT2-attenuated (*ZnT2KD*) cells. Merged images illustrate co-localization of β-casein and V-ATPase (*yellow*). Nuclei were counterstained with DAPI (*blue*). *Scale bar*, 20 μm. *B,* data represent mean Pearson's coefficient ± S.D. calculated from all cells in five random images (×63)/group from three independent experiments; ***, $p < 0.001$. *C,* representative confocal images of GFP-tagged β-casein (*green*) in mock-transfected (*Control*), ZnT2-attenuated (*ZnT2KD*), V-ATPase-attenuated (*V-ATPase KD*) cells, and cells treated with Bafilomycin A1 (+*BafA1*) or TPEN (+*TPEN*), and ZnT2KD cells treated with TPEN (*ZnT2KD+TPEN*). Cells were imaged prior to or 15, 30, and 60 min following prolactin treatment. Note perinuclear accumulation of GFP-tagged β-casein in ZnTKD, +BafA1, V-ATPase KD, and ZnT2KD + TPEN cells. *Scale bar*, 10 μm. *D,* data represent mean lysozyme activity detected in the conditioned medium ± S.D. in 2 replicates/group from three independent experiments; *, $p < 0.05$; **, $p < 0.01$; and ***, $p < 0.001$.

region in ZnT2-attenuated MECs (Fig. 8*C*). This was similar to defects seen in MECs treated with Bafilomycin A1, a specific inhibitor of V-ATPase, and also in V-ATPase-attenuated cells (Fig. 8*C*, Fig. S4). Our data suggest that this defect was not due to cytoplasmic Zn^{2+} accumulation, as β-casein continued to traffic to the cell surface in response to PRL in control cells, and remained perinuclear in ZnT2-attenuated MECs when treated with TPEN (Fig. 8*C*). Again, these findings suggest that the role of ZnT2 in regulating vesicle secretion is independent of its function in Zn^{2+} transport, and are consistent with our findings on the role of Zn^{2+} in the acidification of secretory vesicles. These studies are consistent with the reduction in milk β-casein levels observed in lactating *ZnT2ko* mice, and decreased β-casein secretion into conditioned medium that was previously noted in ZnT2-attenuated MECs (27), and we now propose that these defects may be due to impaired vesicle biogenesis and/or trafficking. This effect was not specific to large β-casein-containing vesicles as we similarly found that lysozyme secretion into conditioned medium was also reduced by ZnT2- and V-ATPase-attenuation and Bafilomycin A1 treatment (Fig. 8*D*). In addition to playing a role in vesicle biogenesis and acidification, ZnT2-mediated Zn^{2+} transport into secretory vesicles might play a direct role in packaging specific components for secretion into milk. For instance, a considerable amount of Zn^{2+} binds to caseins to allow the maturation into casein micelles (86–88). It is likely that other constituents of secretory vesicles in the MECs may be influenced by the absence of vesicular Zn^{2+}, including lactoferrin (89, 90), immunoglobulin A (90), and lysozyme (91). In addition, Lavoie *et al.* (92) showed that vesicular Zn^{2+} is required for calcium-stimulated vesicle trafficking. Thus, the loss of ZnT2 function may interfere with secretion in MECs by impairing 1) biogenesis; 2) acidification; 3) packaging; and/or 4) trafficking of secretory vesicles to the cell surface.

In summary, this study provides four principal sets of observations on the functional role of ZnT2 in the establishment of secretory function in MECs (Fig. 9). We demonstrated that 1) ZnT2-mediated Zn^{2+} transport regulates PTEN stability and activity, which is required for establishing MEC polarity and luminal development; 2) the establishment of polarity in MECs is required for PRLR trafficking and thus PRL signaling; 3) V-ATPase and vesicle acidification are required for secretory function in MECs; and 4) V-ATPase and ZnT2 directly interact to facilitate proton transport, vesicle acidification, and secre-

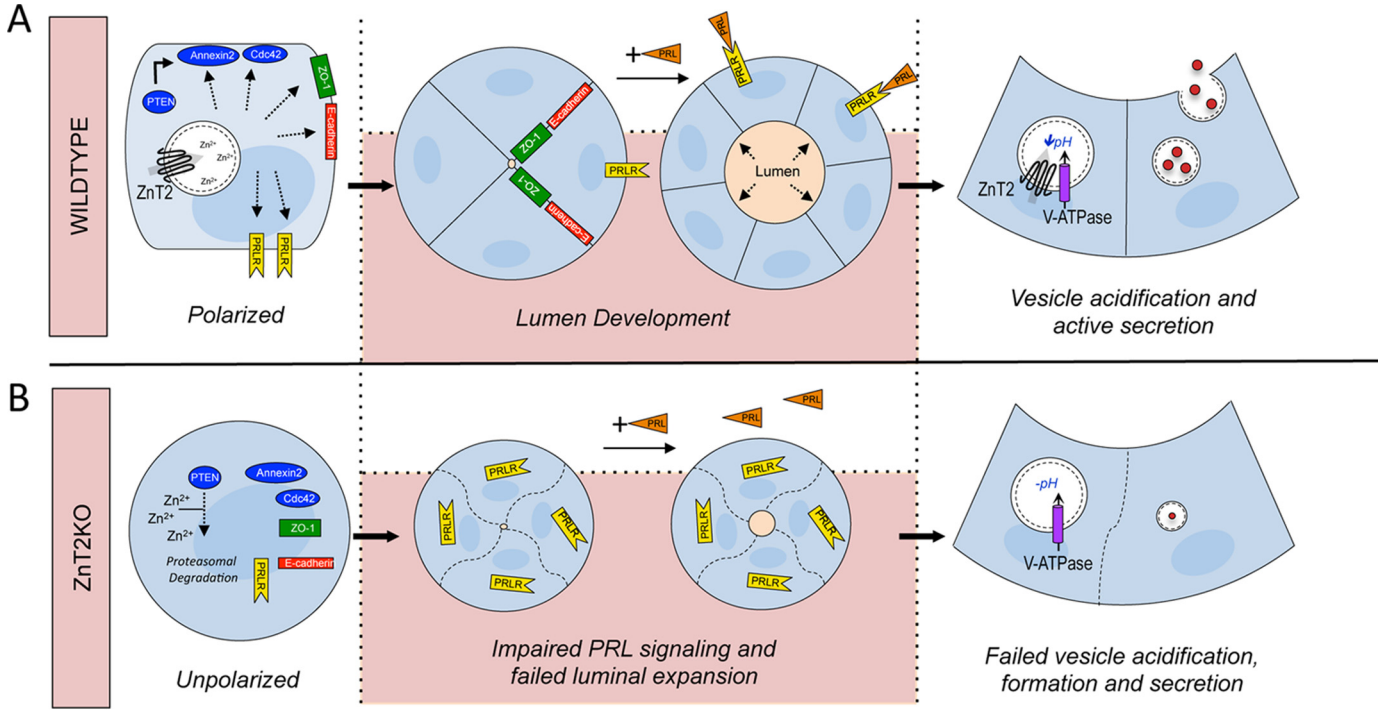

Figure 9. A model describing the functional consequence of loss of ZnT2-mediated Zn^{2+} homeostasis on epithelial polarity, lumen development and secretory function. *A,* in cells expressing ZnT2 (*Wildtype*), Zn^{2+} homeostasis is maintained by ZnT2-mediated Zn^{2+} vesicularization. To establish epithelial polarity, PTEN recruits membrane proteins, Annexin2, which then recruits Cdc42. When cells are grown in 3D and treated with prolactin, polarity is established and lumen development occurs. Cell-cell junctions form (E-cadherin and ZO-1) and membrane trafficking of PRLR occurs. ZnT2 interacts with V-ATPase to acidify vesicles for secretory vesicle formation, trafficking, and secretion into the lumen. *B,* in ZnT2-attenuated cells (*ZnT2KD*), loss of ZnT2-mediated Zn^{2+} transport increases cytoplasmic Zn^{2+} and degrades PTEN through the proteasomal pathway, which impairs PTEN-mediated membrane recruitment of Annexin2 and Cdc4 and disrupts epithelial polarization. ZnT2KD cells fail to form cell-cell junctions and fail to traffic PRLR to the cell surface. Consequently, when cells are grown in 3D and treated with prolactin, polarity is impaired and vesicle biogenesis, acidification, and secretion are compromised, disrupting secretory function.

tion. Moreover, defects in ZnT2 function in the mammary gland may have broader health implications beyond lactation. For example, impairments in MEC polarity drives breast tumorigenesis (93–95). In addition, vesicle biogenesis/trafficking may promote sustained activation of key growth and developmental pathways such as those mediated through EGFR (65), Notch, and TGF-β signaling (20), which also contribute to breast tumorigenesis (96–98). Although we previously proposed a role for ZnT2-mediated Zn^{2+} homeostasis in regulating breast tumor development (99), further studies are required to explore this relationship.

Experimental procedures

Mice

All animal experiments were approved by the Institutional Animal Care and Use Committee at the Pennsylvania State University, which is accredited by the American Association for the Accreditation of Laboratory Animal Care. Wild-type (*wt*) and ZnT2-null (*ZnT2ko*) mice were generated as previously described (27). Mice were housed in polycarbonate-ventilated cages and fed a standard commercial rodent diet (LabDiet, Quakertown, PA) *ad libitum*. They were maintained on a 12-h light/dark cycle under controlled temperature and humidity. To study the role of ZnT2 in the mammary gland on secretory function, *wt* and *ZnT2ko* female mice were mated with a *wt* male (2:1 ratio) for 2 weeks, allowed to deliver naturally and nurse their litters up to lactation day (LD) 10. Mice were euthanized by CO_2 asphyxiation and tissues were immediately excised and fixed in 4% paraformaldehyde or Karnovsky's fixative for further analyses.

Histological analysis

Mammary glands were fixed in 4% paraformaldehyde in phosphate-buffered saline (PBS) overnight, embedded in paraffin, and sections (5 μm) were stained with hematoxylin and eosin (H&E) or immunostained as previously described (27). The following antibodies were used for immunostaining: anti-E-cadherin (adherence junction protein, 1:50; Sigma), anti-zonula occludens-1 (ZO-1, tight junction protein, 1 μg/ml; Abcam, Cambridge, MA), anti-ATP6V0A2 (V0a domain, 1 μg/μl; Sigma), and anti-V-ATPase B1/2 (V1 domain, 1:200; Santa Cruz Biotechnology). Antibodies were either visualized with Vectastain ABC Kit (Vector Labs, Burlingame, CA) and then counterstained with toluidine blue (E-cadherin), or with Alexa Fluor® 488 (ZO-1 and V-ATPase) and then counterstained with DAPI nuclear stain (Thermo Fisher Scientific, Waltham, MA). Stained sections were examined using the Leica DM IL LED microscope equipped with a digital Leica DFC425 camera (Leica Microsystems, Buffalo Grove, IL), or the Leica SP8 Inverted Confocal Microscope (Leica Microsytems). Lumen area was measured using Adobe Photoshop CS6 in all intact alveoli identified in five random images (×10) from one inguinal mammary gland per mouse (n = 4 mice/genotype). Defective expansion in *ZnT2ko* mice or ZnT2KD cells was indi-

cated when an alveoli had a luminal area smaller than the smallest luminal area identified in *wt* mice or ZnT2-expressing mammospheres. The percent of alveoli with expanded lumen was calculated as the number of mature alveoli/total number alveoli in five random images (×10) at ×100%.

Transmission electron microscopy

Excised mammary glands were immediately harvested in Karnovsy's fixative (4% paraformaldehyde, 1 M sodium hydroxide, 25% glutaraldehyde, 0.2 M sodium cacodylate, pH 7.3) for 24 h and stored in sodium cacodylate (0.1 mM) until processed and imaged as previously described (27) using a JEOL JEM1400 Digital Capture Transmission Electron Microscope at the Penn State Hershey College of Medicine Imaging Facility.

Cell culture and transfection

Mouse MECs (HC11 cells) were a gift from Dr. Jeffery Rosen (Baylor College of Medicine, Houston, TX) and used with permission of Dr. Bernd Groner (Institute for Biomedical Research, Frankford, Germany). HC11 cells were maintained in growth medium (RPMI 1640 supplemented with 10% fetal bovine serum, insulin (5 μg/ml), epidermal growth factor (10 ng/ml), and gentamycin). ZnT2 or V-ATPase was attenuated by transfecting cells with siRNA targeted against ZnT2 (5′-CCAUCUGCCUGGUGUUCAU-3; Sigma) or ATP6V0A2 (V-ATPase subunit V0; (SASI_Mm01_00029260; Sigma) using Lipofectamine 2000 (Thermo Fisher) as previously described (100). Cells were differentiated with prolactin (PRL; 1 μg/ml) and cortisol (2 μM) for 24 h where indicated. Cells were pretreated with cycloheximide (10 μM for up to 3 h) to inhibit protein translation, MG132 (10 μM for 3 h) to inhibit proteasomal degradation, TPEN (10 μM for 2 h) to selectively chelate Zn^{2+}, or Bafilomycin A1 (10 μM for 1 h) to specifically inhibit V-ATPase, where indicated.

Mammospheres in 3D culture

HC11 cells were plated on coverslips coated with 50 μl of growth factor-reduced Matrigel® (Corning Life Sciences, Corning, NY). After attachment on Matrigel®, cells were transfected with ZnT2 siRNA as described above. Cells were maintained in growth medium for 2–3 days and then treated with differentiation medium (1 μg/ml of PRL, 2 μM cortisol, 5 μg/ml of insulin) for 4 days to differentiate and form alveoli. Mammospheres were fixed in 4% paraformaldehyde for 10 min at room temperature and permeabilized with 0.5% Triton X-100/PBS for 10 min at 4 °C. After three rinses with 100 mM glycine/PBS, the mammospheres were blocked with immunofluorescence (IF) buffer (130 mM NaCl, 7 mM Na_2HPO_4, 3.5 mM NaH_2PO_4, 7.7 mM NaN_3, 0.1% BSA, 0.2% Triton X-100, 0.05% Tween 20) containing 10% goat serum, and then incubated with primary antibody (anti-mouse ZO-1; 5 μg/ml) diluted in IF buffer containing 10% goat serum overnight at 4 °C. Following three 15-min washes with IF buffer, mammospheres were incubated with secondary antibody (goat anti-mouse IgG labeled with Alexa Fluor® 488) for 1 h at room temperature. Following three 15-min washes with IF buffer, nuclei were counterstained with DAPI nuclear stain (0.5 ng/ml) diluted in PBS for 15 min at room temperature. Mammospheres were mounted with Prolong Diamond Reagent (Thermo Fisher) and examined using the Leica Inverted Confocal Microscope SP8. Alveolar area (total mammosphere size) and diameter (lumen size) were measured using Adobe Photoshop CS6 in five random intact mammospheres/group imaged at ×20.

Immunofluorescence

HC11 cells were immunostained as previously described (29). Briefly, cells were fixed with 4% paraformaldehyde for 10 min, permeabilized with 0.2% Triton X-100 for 10 min, and stained with the following antibodies: anti-E-cadherin (1:50), anti-ZO-1 (5 μg/ml), anti-annexin 2 (Axn2; 1:50; Santa Cruz Biotechnology), anti-V-ATPase a0 (1 μg/μl); anti-V-ATPase B1/2 (1:200), anti-PRLR (5 μg/ml; Invitrogen), anti-β-casein (1:200; Santa Cruz), PKH26 (1:500; Sigma) or anti-HA (1:1000; Sigma). Primary antibodies were visualized using secondary antibodies conjugated with Alexa Fluor® 488 or Alexa Fluor® 568, counterstained with DAPI nuclear stain, and mounted with Prolong Diamond Reagent. Slides were examined using the Leica SP8Inverted Confocal Microscope.

Immunoblotting

Tissue and cell lysates were homogenized in buffer (20 mM HEPES, 1 mM EDTA, 250 mM sucrose, pH 7.4) containing protease inhibitors and the total cell lysate or membrane fractions were prepared as previously described (101). Proteins were separated by SDS-PAGE electrophoresis and transferred onto nitrocellulose membrane. The following antibodies were used: anti-PTEN (1:200; Santa Cruz Biotechnology), anti-PRLR (5 μg/ml), anti-Cdc42 (1:1000; Cell Signaling, Danvers, MA), anti-p-AKT (1:1000; Cell Signaling), anti-AKT (1:1000; Cell Signaling), anti-ATP6V0A2 (1 μg/μl), and anti-V-ATPase B1/2 (1:200). Antibodies were detected with horseradish peroxidase-conjugated anti-rabbit, -mouse, or -goat IgG (Thermo Fisher Scientific). Membranes were stripped before re-probing with another antibody or β-actin (1:5000, Sigma) as loading or normalization controls where indicated. Protein was detected with a SuperSignal Femto Chemiluminescent Detection System (Thermo Fisher Scientific) and imaged using digital imaging (FluorChem M, Cell Biosciences, USA). Band signal intensity was quantified using AlphaView software (ProteinSimple, San Jose, CA). All spliced images were from a single immunoblot; the area of vertical splicing was indicated with a dotted line.

Cell-surface biotinylation of PRLR

N-Hydroxysulfosuccinimide biotin (Thermo Fisher Scientific) was used to label cell-surface proteins to detect PRLR at the cell surface as described previously (32). Biotinylated proteins were eluted by heating to 95 °C in Laemmli buffer containing 100 mM dithiothreitol, electrophoresed using SDS-PAGE, transferred to nitrocellulose membrane, and immunoblotted with anti-PRLR antibody (5 μg/ml) as described above. Protein was detected with SuperSignal Femto Chemiluminescent Detection System and imaged using digital imaging. Band signal intensity was quantified using AlphaView software.

Membrane recruitment of Cdc42

HC11 cell lysates were collected in homogenization buffer, sonicated briefly, centrifuged at 500 × *g* for 5 min to remove debris, and a sample of supernatant (cell lysate) was set aside (total). The supernatant was further centrifuged at 100,000 × *g* for 30 min to pellet the total membrane fraction and isolate the cytosolic fraction. Cell lysate, cytosolic and membrane fractions (20 μg) were loaded on a 10% SDS-polyacrylamide gel and immunoblotted for Cdc42 to assess the recruitment of Cdc42 to the membrane, as described above. Ponceau staining was used as loading control.

Secretory function

Large vesicles—To monitor the secretion of large (~1 μm) vesicles, HC11 cells were plated on a 24-well plate, grown until ~80% confluent, and transfected with plasmid (0.8 μg/well) containing Green Fluorescent Protein (GFP)-tagged β-casein (Cambridge Bioscience, Cambridge, UK). Cells were pretreated with cycloheximide (100 μg/ml) and held at room temperature (20 °C) for 3 h to stop protein translation, and then treated with PRL (1 μg/ml) and cortisol (2 μM) for up to 60 min to stimulate secretion. In some experiments, cells were pretreated with TPEN (10 μM for 2 h). Cells were fixed as described above and GFP-tagged β-casein was imaged at discrete time points (0, 15, 30, and 60 min).

Small vesicles—To monitor the secretion of small (~200 nm) vesicles, HC11 cells were grown on 96-well plates and differentiated with PRL (1 μg/ml) and cortisol (2 μM) for 24 h. Medium was removed and then cells were treated for an additional 12 h with PRL (1 μg/ml) and cortisol (2 μM) and either Bafilomycin A1 (1 μM in DMSO) or DMSO (control). Conditioned medium was collected and assayed for lysozyme activity using EnzChek® Lysozyme Assay Kit (Thermo Fisher Scientific) according to the manufacturer's instructions.

Immunoprecipitation

HC11 cells were cultured in 6-well dishes, washed in ice-cold PBS, and lysed with radioimmunoprecipitation (RIPA) buffer for 5 min on ice. Cells were scraped into microcentrifuge tubes and sonicated on ice, then centrifuged for 10 min at 14,000 × *g* at 4 °C. The protein concentration of the clarified supernatants was determined using the Bradford assay. Lysates were incubated with 5 μg of antibody (anti-HA, -V0, or -V1) for 3 h followed by Protein A-agarose beads (Sigma) for 1 h at 4 °C with rotation. The resin was pelleted by centrifugation at 10,000 × *g* for 1 min and washed four times with RIPA buffer. Following the final wash, sample buffer was added to the resin and proteins were eluted and denatured by heating at 95 °C for 5 min. Samples were vortexed and centrifuged at 10,000 × *g* for 5 min to pellet the resin. Supernatants were loaded onto a 10% polyacrylamide gel and immunoblotting was performed as described above. Total cell lysates were used as an input control.

Vesicle pH

Vesicle pH was measured using Lysosensor Blue/Yellow DND-160 (Thermo Fisher Scientific). HC11 cells were loaded with Lysosensor Blue/Yellow DND-160 (5 μM diluted in Opti-MEM) for 1 h at 37 °C. After a brief rinse with PBS, cells were imaged using a Leica SP8 inverted confocal microscope. The cells were excited at 405 nm and emitted at two different wavelengths: 455 nm for Lysosensor Blue (channel 1; pH 9) and 540 nm for Lysosensor Yellow (channel 2; pH 3). Imaris 8.2 software (Bitplane, Belfast, UK) was used to measure the fluorescence intensity from channels 1 and 2. The fluorescence intensity from channels 1 and 2 was measured in all vesicles identified in 5 randomly selected cells/image (×63), from 5 images/group. Results were presented as the mean ratio of the fluorescence intensity from channel 1 divided by channel 2 (*i.e.* blue/yellow). Vesicle pH was determined using a calibration curve constructed by adding 5 μM Lysosensor Blue/Yellow DND-160 to Opti-MEM medium held at a specific pH ranging from 4 to 5.5 (in 0.1 increments) and measuring the fluorescence emitted at ~535 nm following excitation at ~340 (blue) and ~380 nm (yellow). The calibration curve was obtained by taking the ratio of emitted fluorescence at the two-excitation wavelengths (*i.e.* blue/yellow) and plotting the fluorescence ratio against the pH. The size and number of all acidic vesicles in a cell were measured in 4 randomly selected cells/image (×63) from 4 images/group using Adobe Photoshop CS6.

Statistical analysis

Results are presented as mean ± S.D. unless otherwise noted. All experiments were performed with at least 2–3 replicates, and all experiments were repeated at least three times. Statistical comparisons were performed using two-tailed Student's *t* tests or one-way analysis of variance with Bonferroni's post hoc test for multiple comparisons (Prism GraphPad). Statistical significance was demonstrated at $p < 0.05$.

Author contributions—S. L. and S. L. K. designed the study. S. L. performed and analyzed the experiments, prepared all the figures, and wrote the manuscript. O. C. R. performed and analyzed the experiments. S. L. K. supervised the experimental work and edited the manuscript. All authors reviewed the results and approved the final version of the manuscript.

Acknowledgment—We thank the Microscopy Imaging Facility, Section of Research Resources, Penn State Hershey College of Medicine for confocal and transmission electron microscopy.

References

1. Crivellato, E., Nico, B., Gallo, V. P., and Ribatti, D. (2010) Cell secretion mediated by granule-associated vesicle transport: a glimpse at evolution. *Anat. Rec.* **293,** 1115–1124
2. Bryant, D. M., and Mostov, K. E. (2008) From cells to organs: building polarized tissue. *Nat. Rev. Mol. Cell Biol.* **9,** 887–901
3. Lavialle, F., Rainteau, D., Massey-Harroche, D., and Metz, F. (2000) Establishment of plasma membrane polarity in mammary epithelial cells correlates with changes in prolactin trafficking and in annexin VI recruitment to membranes. *Biochim. Biophys. Acta* **1464,** 83–94
4. Rodriguez-Boulan, E., and Macara, I. G. (2014) Organization and execution of the epithelial polarity programme. *Nat. Rev. Mol. Cell Biol.* **15,** 225–242
5. Roignot, J., Peng, X., and Mostov, K. (2013) Polarity in mammalian epithelial morphogenesis. *Cold Spring Harbor Perspect. Biol.* **5,** pii.a013789
6. Oakes, S. R., Hilton, H. N., and Ormandy, C. J. (2006) The alveolar switch: coordinating the proliferative cues and cell fate decisions that drive the

formation of lobuloalveoli from ductal epithelium. *Breast Cancer Res.* **8,** 207
7. Whyte, J., Thornton, L., McNally, S., McCarthy, S., Lanigan, F., Gallagher, W. M., Stein, T., and Martin, F. (2010) PKCζ regulates cell polarisation and proliferation restriction during mammary acinus formation. *J. Cell Sci.* **123,** 3316–3328
8. Datta, A., Bryant, D. M., and Mostov, K. E. (2011) Molecular regulation of lumen morphogenesis. *Curr. Biol.* **21,** R126–R136
9. Furuse, M. (2010) Molecular basis of the core structure of tight junctions. *Cold Spring Harbor Perspect. Biol.* **2,** a002907
10. Macara, I. G. (2004) Parsing the polarity code. *Nat. Rev. Mol. Cell Biol.* **5,** 220–231
11. Druso, J. E., Endo, M., Lin, M. C., Peng, X., Antonyak, M. A., Meller, S., and Cerione, R. A. (2016) An essential role for Cdc42 in the functioning of the adult mammary gland. *J. Biol. Chem.* **291,** 8886–8895
12. Shore, A. N., Chang, C. H., Kwon, O. J., Weston, M. C., Zhang, M., Xin, L., and Rosen, J. M. (2016) PTEN is required to maintain luminal epithelial homeostasis and integrity in the adult mammary gland. *Dev. Biol.* **409,** 202–217
13. Hiesinger, P. R., Fayyazuddin, A., Mehta, S. Q., Rosenmund, T., Schulze, K. L., Zhai, R. G., Verstreken, P., Cao, Y., Zhou, Y., Kunz, J., and Bellen, H. J. (2005) The v-ATPase V0 subunit a1 is required for a late step in synaptic vesicle exocytosis in *Drosophila*. *Cell* **121,** 607–620
14. Moore, H. P., Andresen, J. M., Eaton, B. A., Grabe, M., Haugwitz, M., Wu, M. M., and Machen, T. E. (2002) Biosynthesis and secretion of pituitary hormones: dynamics and regulation. *Arch. Physiol. Biochem.* **110,** 16–25
15. Tarasenko, A. S., Sivko, R. V., Krisanova, N. V., Himmelreich, N. H., and Borisova, T. A. (2010) Cholesterol depletion from the plasma membrane impairs proton and glutamate storage in synaptic vesicles of nerve terminals. *J. Mol. Neurosci.* **41,** 358–367
16. Wu, M. M., Grabe, M., Adams, S., Tsien, R. Y., Moore, H. P., and Machen, T. E. (2001) Mechanisms of pH regulation in the regulated secretory pathway. *J. Biol. Chem.* **276,** 33027–33035
17. Forgac, M. (2007) Vacuolar ATPases: rotary proton pumps in physiology and pathophysiology. *Nat. Rev. Mol. Cell Biol.* **8,** 917–929
18. Marshansky, V., and Futai, M. (2008) The V-type H+-ATPase in vesicular trafficking: targeting, regulation and function. *Curr. Opin. Cell Biol.* **20,** 415–426
19. Hennigar, S. R., Seo, Y. A., Sharma, S., Soybel, D. I., and Kelleher, S. L. (2015) ZnT2 is a critical mediator of lysosomal-mediated cell death during early mammary gland involution. *Sci. Rep.* **5,** 8033
20. Pamarthy, S., Mao, L., Katara, G. K., Fleetwood, S., Kulshreshta, A., Gilman-Sachs, A., and Beaman, K. D. (2016) The V-ATPase a2 isoform controls mammary gland development through Notch and TGF-β signaling. *Cell Death Dis* **7,** e2443
21. Triplett, A. A., Sakamoto, K., Matulka, L. A., Shen, L., Smith, G. H., and Wagner, K. U. (2005) Expression of the whey acidic protein (Wap) is necessary for adequate nourishment of the offspring but not functional differentiation of mammary epithelial cells. *Genesis* **43,** 1–11
22. Wagner, K. U., Young, W. S., 3rd, Liu, X., Ginns, E. I., Li, M., Furth, P. A., and Hennighausen, L. (1997) Oxytocin and milk removal are required for post-partum mammary-gland development. *Genes Funct.* **1,** 233–244
23. Watkin, H., Richert, M. M., Lewis, A., Terrell, K., McManaman, J. P., and Anderson, S. M. (2008) Lactation failure in Src knockout mice is due to impaired secretory activation. *BMC Dev. Biol.* **8,** 6
24. Zhang, L., Reidy, S. P., Bogachev, O., Hall, B. K., Majdalawieh, A., and Ro, H. S. (2011) Lactation defect with impaired secretory activation in AEBP1-null mice. *PLoS ONE* **6,** e27795
25. Hennigar, S. R., Velasquez, V., and Kelleher, S. L. (2015) Obesity-induced inflammation is associated with alterations in subcellular zinc pools and premature mammary gland involution in lactating mice. *J. Nutr.* **145,** 1999–2005
26. Itsumura, N., Inamo, Y., Okazaki, F., Teranishi, F., Narita, H., Kambe, T., and Kodama, H. (2013) Compound heterozygous mutations in SLC30A2/ZnT2 results in low milk zinc concentrations: a novel mechanism for zinc deficiency in a breast-fed infant. *PLoS ONE* **8,** e64045
27. Lee, S., Hennigar, S. R., Alam, S., Nishida, K., and Kelleher, S. L. (2015) Essential role for zinc transporter 2 (ZnT2)-mediated zinc transport in mammary gland development and function during lactation. *J. Biol. Chem.* **290,** 13064–13078
28. McCormick, N. H., and Kelleher, S. L. (2012) ZnT4 provides zinc to zinc-dependent proteins in the trans-Golgi network critical for cell function and Zn export in mammary epithelial cells. *Am. J. Physiol. Cell Physiol.* **303,** C291–C297
29. Alam, S., Hennigar, S. R., Gallagher, C., Soybel, D. I., and Kelleher, S. L. (2015) Exome sequencing of SLC30A2 identifies novel loss- and gain-of-function variants associated with breast cell dysfunction. *J. Mammary Gland Biol. Neoplasia* **20,** 159–172
30. Lasry, I., Golan, Y., Berman, B., Amram, N., Glaser, F., and Assaraf, Y. G. (2014) In situ dimerization of multiple wild type and mutant zinc transporters in live cells using bimolecular fluorescence complementation. *J. Biol. Chem.* **289,** 7275–7292
31. Kelleher, S. L., and Lönnerdal, B. (2003) Zn transporter levels and localization change throughout lactation in rat mammary gland and are regulated by Zn in mammary cells. *J. Nutr.* **133,** 3378–3385
32. Lopez, V., and Kelleher, S. L. (2009) Zinc transporter-2 (ZnT2) variants are localized to distinct subcellular compartments and functionally transport zinc. *Biochem. J.* **422,** 43–52
33. Palmiter, R. D., Cole, T. B., and Findley, S. D. (1996) ZnT-2, a mammalian protein that confers resistance to zinc by facilitating vesicular sequestration. *EMBO J.* **15,** 1784–1791
34. Kelleher, S. L., McCormick, N. H., Velasquez, V., and Lopez, V. (2011) Zinc in specialized secretory tissues: roles in the pancreas, prostate, and mammary gland. *Adv. Nutr.* **2,** 101–111
35. Lichten, L. A., and Cousins, R. J. (2009) Mammalian zinc transporters: nutritional and physiologic regulation. *Annu Rev Nutr* **29,** 153–176
36. Chowanadisai, W., Lönnerdal, B., and Kelleher, S. L. (2006) Identification of a mutation in SLC30A2 (ZnT-2) in women with low milk zinc concentration that results in transient neonatal zinc deficiency. *J. Biol. Chem.* **281,** 39699–39707
37. Miletta, M. C., Bieri, A., Kernland, K., Schöni, M. H., Petkovic, V., Flück, C. E., Eblé, A., and Mullis, P. E. (2013) Transient neonatal zinc deficiency caused by a heterozygous G87R mutation in the zinc transporter ZnT-2 (SLC30A2) gene in the mother highlighting the importance of Zn^{2+} for normal growth and development. *Int. J. Endocrinol.* **2013,** 259189
38. Dórea, J. G. (2002) Zinc deficiency in nursing infants. *J. Am. Coll. Nutr.* **21,** 84–87
39. Piela, Z., Szuber, M., Mach, B., and Janniger, C. K. (1998) Zinc deficiency in exclusively breast-fed infants. *Cutis* **61,** 197–200
40. Noatynska, A., Tavernier, N., Gotta, M., and Pintard, L. (2013) Coordinating cell polarity and cell cycle progression: what can we learn from flies and worms? *Open Biol.* **3,** 130083
41. Hartmann, P. E., and Kulski, J. K. (1978) Changes in the composition of the mammary secretion of women after abrupt termination of breast feeding. *J. Physiol.* **275,** 1–11
42. Morton, J. A. (1994) The clinical usefulness of breast milk sodium in the assessment of lactogenesis. *Pediatrics* **93,** 802–806
43. Semba, R. D., Kumwenda, N., Taha, T. E., Hoover, D. R., Lan, Y., Eisinger, W., Mtimavalye, L., Broadhead, R., Miotti, P. G., Van Der Hoeven, L., and Chiphangwi, J. D. (1999) Mastitis and immunological factors in breast milk of lactating women in Malawi. *Clin Diagn Lab Immunol* **6,** 671–674
44. Nagaoka, K., Zhang, H., Watanabe, G., and Taya, K. (2013) Epithelial cell differentiation regulated by MicroRNA-200a in mammary glands. *PLoS ONE* **8,** e65127
45. Xu, R., Nelson, C. M., Muschler, J. L., Veiseh, M., Vonderhaar, B. K., and Bissell, M. J. (2009) Sustained activation of STAT5 is essential for chromatin remodeling and maintenance of mammary-specific function. *J. Cell Biol.* **184,** 57–66
46. Xu, R., Spencer, V. A., Groesser, D. L., and Bissell, M. J. (2010) Laminin regulates PI3K basal localization and activation to sustain STAT5 activation. *Cell Cycle* **9,** 4315–4322

47. Jäger, R., Pappas, L., and Schorle, H. (2008) Lactogenic differentiation of HC11 cells is not accompanied by downregulation of AP-2 transcription factor genes. *BMC Res. Notes* **1,** 29
48. Xian, W., Schwertfeger, K. L., Vargo-Gogola, T., and Rosen, J. M. (2005) Pleiotropic effects of FGFR1 on cell proliferation, survival, and migration in a 3D mammary epithelial cell model. *J. Cell Biol.* **171,** 663–673
49. Martin-Belmonte, F., Gassama, A., Datta, A., Yu, W., Rescher, U., Gerke, V., and Mostov, K. (2007) PTEN-mediated apical segregation of phosphoinositides controls epithelial morphogenesis through Cdc42. *Cell* **128,** 383–397
50. Leslie, N. R., Batty, I. H., Maccario, H., Davidson, L., and Downes, C. P. (2008) Understanding PTEN regulation: PIP2, polarity and protein stability. *Oncogene* **27,** 5464–5476
51. Zhou, J., and Parada, L. F. (2009) A motor driving PTEN. *Nat. Cell. Biol.* **11,** 1177–1179
52. Nagaoka, K., Udagawa, T., and Richter, J. D. (2012) CPEB-mediated ZO-1 mRNA localization is required for epithelial tight-junction assembly and cell polarity. *Nat. Commun.* **3,** 675
53. Kroschewski, R., Hall, A., and Mellman, I. (1999) Cdc42 controls secretory and endocytic transport to the basolateral plasma membrane of MDCK cells. *Nat. Cell. Biol.* **1,** 8–13
54. Bray, K., Gillette, M., Young, J., Loughran, E., Hwang, M., Sears, J. C., and Vargo-Gogola, T. (2013) Cdc42 overexpression induces hyperbranching in the developing mammary gland by enhancing cell migration. *Breast Cancer Res.* **15,** R91
55. Dupont, J., Renou, J. P., Shani, M., Hennighausen, L., and LeRoith, D. (2002) PTEN overexpression suppresses proliferation and differentiation and enhances apoptosis of the mouse mammary epithelium. *J. Clin. Invest.* **110,** 815–825
56. Wang, Z., Hou, X., Qu, B., Wang, J., Gao, X., and Li, Q. (2014) Pten regulates development and lactation in the mammary glands of dairy cows. *PLoS ONE* **9,** e102118
57. Berglund, F. M., Weerasinghe, N. R., Davidson, L., Lim, J. C., Eickholt, B. J., and Leslie, N. R. (2013) Disruption of epithelial architecture caused by loss of PTEN or by oncogenic mutant p110α/PIK3CA but not by HER2 or mutant AKT1. *Oncogene* **32,** 4417–4426
58. Langlois, M. J., Bergeron, S., Bernatchez, G., Boudreau, F., Saucier, C., Perreault, N., Carrier, J. C., and Rivard, N. (2010) The PTEN phosphatase controls intestinal epithelial cell polarity and barrier function: role in colorectal cancer progression. *PLoS ONE* **5,** e15742
59. Wang, J., Zhu, H. H., Chu, M., Liu, Y., Zhang, C., Liu, G., Yang, X., Yang, R., and Gao, W. Q. (2014) Symmetrical and asymmetrical division analysis provides evidence for a hierarchy of prostate epithelial cell lineages. *Nat. Commun.* **5,** 4758
60. Chalhoub, N., and Baker, S. J. (2009) PTEN and the PI3-kinase pathway in cancer. *Annu. Rev. Pathol.* **4,** 127–150
61. Song, M. S., Salmena, L., and Pandolfi, P. P. (2012) The functions and regulation of the PTEN tumour suppressor. *Nat. Rev. Mol. Cell Biol.* **13,** 283–296
62. Xie, Y., Naizabekov, S., Chen, Z., and Tokay, T. (2016) Power of PTEN/AKT: Molecular switch between tumor suppressors and oncogenes. *Oncol. Lett.* **12,** 375–378
63. Wu, W., Wang, X., Zhang, W., Reed, W., Samet, J. M., Whang, Y. E., and Ghio, A. J. (2003) Zinc-induced PTEN protein degradation through the proteasome pathway in human airway epithelial cells. *J. Biol. Chem.* **278,** 28258–28263
64. Kwak, Y. D., Wang, B., Pan, W., Xu, H., Jiang, X., and Liao, F. F. (2010) Functional interaction of phosphatase and tensin homologue (PTEN) with the E3 ligase NEDD4–1 during neuronal response to zinc. *J. Biol. Chem.* **285,** 9847–9857
65. Shinde, S. R., and Maddika, S. (2016) PTEN modulates EGFR late endocytic trafficking and degradation by dephosphorylating Rab7. *Nat. Commun.* **7,** 10689
66. Neville, M. C., McFadden, T. B., and Forsyth, I. (2002) Hormonal regulation of mammary differentiation and milk secretion. *J. Mammary Gland Biol. Neoplasia* **7,** 49–66
67. Qian, L., Lopez, V., Seo, Y. A., and Kelleher, S. L. (2009) Prolactin regulates ZNT2 expression through the JAK2/STAT5 signaling pathway in mammary cells. *Am. J. Physiol. Cell Physiol.* **297,** C369–C377
68. Truchet, S., and Ollivier-Bousquet, M. (2009) Mammary gland secretion: hormonal coordination of endocytosis and exocytosis. *Animal* **3,** 1733–1742
69. Stiernet, P., Guiot, Y., Gilon, P., and Henquin, J. C. (2006) Glucose acutely decreases pH of secretory granules in mouse pancreatic islets: mechanisms and influence on insulin secretion. *J. Biol. Chem.* **281,** 22142–22151
70. Collaco, A. M., Geibel, P., Lee, B. S., Geibel, J. P., and Ameen, N. A. (2013) Functional vacuolar ATPase (V-ATPase) proton pumps traffic to the enterocyte brush border membrane and require CFTR. *Am. J. Physiol. Cell Physiol* **305,** C981–C996
71. Michel, V., Licon-Munoz, Y., Trujillo, K., Bisoffi, M., and Parra, K. J. (2013) Inhibitors of vacuolar ATPase proton pumps inhibit human prostate cancer cell invasion and prostate-specific antigen expression and secretion. *Int. J. Cancer* **132,** E1–E10
72. Melnik, V. I., Bikbulatova, L. S., Gulyaeva, N. V., and Bazyan, A. S. (2001) Synaptic vesicle acidification and exocytosis studied with acridine orange fluorescence in rat brain synaptosomes. *Neurochem. Res.* **26,** 549–554
73. Zimmermann, B., Dames, P., Walz, B., and Baumann, O. (2003) Distribution and serotonin-induced activation of vacuolar-type H^+-ATPase in the salivary glands of the blowfly *Calliphora vicina*. *J. Exp. Biol.* **206,** 1867–1876
74. Breton, S., and Brown, D. (2007) New insights into the regulation of V-ATPase-dependent proton secretion. *Am. J. Physiol. Renal Physiol* **292,** F1–F10
75. Nishi, T., and Forgac, M. (2002) The vacuolar H^+-ATPases–nature's most versatile proton pumps. *Nat. Rev. Mol. Cell Biol.* **3,** 94–103
76. Kane, P. M. (1995) Disassembly and reassembly of the yeast vacuolar H^+-ATPase *in vivo*. *J. Biol. Chem.* **270,** 17025–17032
77. Sautin, Y. Y., Lu, M., Gaugler, A., Zhang, L., and Gluck, S. L. (2005) Phosphatidylinositol 3-kinase-mediated effects of glucose on vacuolar H^+-ATPase assembly, translocation, and acidification of intracellular compartments in renal epithelial cells. *Mol. Cell. Biol.* **25,** 575–589
78. Naik, H. B., Beshire, M., Walsh, B. M., Liu, J., and Soybel, D. I. (2009) Secretory state regulates Zn^{2+} transport in gastric parietal cell of the rabbit. *Am. J. Physiol. Cell Physiol* **297,** C979–C989
79. Schapiro, F. B., and Grinstein, S. (2000) Determinants of the pH of the Golgi complex. *J. Biol. Chem.* **275,** 21025–21032
80. Fukao, Y., and Ferjani, A. (2011) V-ATPase dysfunction under excess zinc inhibits Arabidopsis cell expansion. *Plant Signal. Behav.* **6,** 1253–1255
81. Cowland, J. B., and Borregaard, N. (2016) Granulopoiesis and granules of human neutrophils. *Immunol. Rev.* **273,** 11–28
82. Tanguy, E., Carmon, O., Wang, Q., Jeandel, L., Chasserot-Golaz, S., Montero-Hadjadje, M., and Vitale, N. (2016) Lipids implicated in the journey of a secretory granule: from biogenesis to fusion. *J. Neurochem.* **137,** 904–912
83. Liu, F., Pawliwec, A., Feng, Z., Yasruel, Z., Lebrun, J. J., and Ali, S. (2015) Prolactin/Jak2 directs apical/basal polarization and luminal linage maturation of mammary epithelial cells through regulation of the Erk1/2 pathway. *Stem Cell Res.* **15,** 376–383
84. Peixoto, E. B., and Collares-Buzato, C. B. (2006) Modulation of the epithelial barrier by dexamethasone and prolactin in cultured Madin-Darby canine kidney (MDCK) cells. *Cell Biol. Int.* **30,** 101–113
85. Stelwagen, K., McFadden, H. A., and Demmer, J. (1999) Prolactin, alone or in combination with glucocorticoids, enhances tight junction formation and expression of the tight junction protein occludin in mammary cells. *Mol. Cell. Endocrinol.* **156,** 55–61
86. Blakeborough, P., Salter, D. N., and Gurr, M. I. (1983) Zinc binding in cow's milk and human milk. *Biochem. J.* **209,** 505–512
87. Harzer, G., and Kauer, H. (1982) Binding of zinc to casein. *Am. J. Clin. Nutr.* **35,** 981–987
88. Singh, H., Flynn, A., and Fox, P. F. (1989) Zinc binding in bovine milk. *J. Dairy Res.* **56,** 249–263

89. Ainscough, E. W., Brodie, A. M., and Plowman, J. E. (1980) Zinc transport by lactoferrin in human milk. *Am. J. Clin. Nutr.* **33,** 1314–1315
90. Pozzi, C. M., Braga, C. P., Vieira, J. C., Cavecci, B., Vitor de Queiroz, J., de Souza Barbosa, H., Arruda, M. A., Gozzo, F. C., and Padilha Pde, M. (2015) Metal ions bound to the human milk immunoglobulin A: metalloproteomic approach. *Food Chem.* **166,** 492–497
91. Chakraborti, S., Chatterjee, T., Joshi, P., Poddar, A., Bhattacharyya, B., Singh, S. P., Gupta, V., and Chakrabarti, P. (2010) Structure and activity of lysozyme on binding to ZnO nanoparticles. *Langmuir* **26,** 3506–3513
92. Lavoie, N., Jeyaraju, D. V., Peralta, M. R., 3rd, Seress, L., Pellegrini, L., and Tóth, K. (2011) Vesicular zinc regulates the Ca^{2+} sensitivity of a subpopulation of presynaptic vesicles at hippocampal mossy fiber terminals. *J. Neurosci.* **31,** 18251–18265
93. McCaffrey, L. M., and Macara, I. G. (2011) Epithelial organization, cell polarity and tumorigenesis. *Trends Cell Biol.* **21,** 727–735
94. Wodarz, A., and Näthke, I. (2007) Cell polarity in development and cancer. *Nat. Cell. Biol.* **9,** 1016–1024
95. Zhan, L., Rosenberg, A., Bergami, K. C., Yu, M., Xuan, Z., Jaffe, A. B., Allred, C., and Muthuswamy, S. K. (2008) Deregulation of scribble promotes mammary tumorigenesis and reveals a role for cell polarity in carcinoma. *Cell* **135,** 865–878
96. Masuda, H., Zhang, D., Bartholomeusz, C., Doihara, H., Hortobagyi, G. N., and Ueno, N. T. (2012) Role of epidermal growth factor receptor in breast cancer. *Breast Cancer Res. Treat* **136,** 331–345
97. Mazzone, M., Selfors, L. M., Albeck, J., Overholtzer, M., Sale, S., Carroll, D. L., Pandya, D., Lu, Y., Mills, G. B., Aster, J. C., Artavanis-Tsakonas, S., and Brugge, J. S. (2010) Dose-dependent induction of distinct phenotypic responses to Notch pathway activation in mammary epithelial cells. *Proc. Natl. Acad. Sci. U.S.A.* **107,** 5012–5017
98. Pang, M. F., Georgoudaki, A. M., Lambut, L., Johansson, J., Tabor, V., Hagikura, K., Jin, Y., Jansson, M., Alexander, J. S., Nelson, C. M., Jakobsson, L., Betsholtz, C., Sund, M., Karlsson, M. C., and Fuxe, J. (2016) TGF-β1-induced EMT promotes targeted migration of breast cancer cells through the lymphatic system by the activation of CCR7/CCL21-mediated chemotaxis. *Oncogene* **35,** 748–760
99. Chandler, P., Kochupurakkal, B. S., Alam, S., Richardson, A. L., Soybel, D. I., and Kelleher, S. L. (2016) Subtype-specific accumulation of intracellular zinc pools is associated with the malignant phenotype in breast cancer. *Mol. Cancer* **15,** 2
100. Seo, Y. A., Lee, S., Hennigar, S. R., and Kelleher, S. L. (2014) Prolactin (PRL)-stimulated ubiquitination of ZnT2 mediates a transient increase in zinc secretion followed by ZnT2 degradation in mammary epithelial cells. *J. Biol. Chem.* **289,** 23653–23661
101. Bostanci, Z., Mack, R. P., Jr., Lee, S., Soybel, D. I., and Kelleher, S. L. (2015) Paradoxical zinc toxicity and oxidative stress in the mammary gland during marginal dietary zinc deficiency. *Reprod. Toxicol.* **54,** 84–92